Chapter I.12

Collective effects

Mauro Migliorati
Sapienza University of Rome, Italy

Particle accelerators use external electromagnetic fields to guide and accelerate charged particles. In a real machine, however, there is another source of electromagnetic fields, the beam itself, which, interacting with the accelerators' devices, produces additional self-induced fields which perturb the particle's motion leading to the so-called collective effects.

The self-induced fields are commonly divided into space charge fields, generated directly by the charge distribution and including the image currents circulating on the walls of a smooth, perfectly conducting pipe, and the wakefields, produced by the finite conductivity of the walls, resonant devices, or any geometrical variation of the beam pipe.

Collective effects in particle accelerators are one of the key constituents for determining the ultimate particle accelerator performance. Their role is becoming increasingly important as particle accelerators are being pushed to ever higher intensity and beam brightness.

Charged particles in a transport channel or in a circular accelerator are confined, guided and accelerated by external electromagnetic (e.m.) fields. Acceleration is usually provided by the electric field of the RF system, while magnetic fields in the dipole magnets are used for guiding the beam on the reference trajectory (orbit), in the quadrupoles for the transverse confinement, and in the sextupoles for the chromaticity correction.

The motion of a single charge q is governed by the Lorentz force through the equation

$$\frac{d(m_0\gamma\mathbf{v})}{dt} = \mathbf{F}^{\text{ext}} = q(\mathbf{E} + \mathbf{v} \times \mathbf{B}) \tag{I.12.1}$$

where m_0 is the rest mass, γ is the relativistic factor, $\mathbf{v}$ is the particle velocity, and $\mathbf{E}$ and $\mathbf{B}$ are the electric and magnetic fields. Observe that we use bold letters for the vectors. The external e. m. fields, used for the beam transport, do not depend on the beam current. With the above equation, we can in principle calculate the trajectory of the charge moving through any e.m. field.

In a real accelerator, however, there is another important source of fields to be considered: the beam itself, which, circulating inside the pipe, produces additional e.m. fields called "self-fields". They depend on the geometry of the beam pipe, the surrounding materials, the charge of the beam, its velocity, and distribution. They are responsible for many phenomena observed in beam dynamics: energy loss, betatron tunes shift, synchronous phase and tune shift, and instabilities. It is customary to divide the self-fields into space charge fields and wakefields. The space charge forces are those generated by the charge

This chapter should be cited as: Collective effects, M. Migliorati, DOI: 10.23730/CYRSP-2024-003.539, in: Proceedings of the Joint Universities Accelerator School (JUAS): Courses and exercises, E. Métral (ed.),
CERN Yellow Reports: School Proceedings, CERN-2024-003, DOI: 10.23730/CYRSP-2024-003, p. 539.

distribution, including the image currents circulating on the walls of a smooth, perfectly conducting pipe. Wakefields are produced by the finite conductivity of the walls, resonant devices, and, more generally, any geometric variation of the beam pipe.

I.12.1 Space Charge

I.12.1.1 Direct space charge forces

Let us consider a relativistic point charge moving, with respect to what we define as our laboratory reference frame, with constant velocity v along the direction s. Observe that, differently from the common Cartesian coordinates, we use here the variable s instead of z. The electric and magnetic fields produced by the charge can be obtained from the relativistic transformation of the electrostatic field of a point charge obtained directly from the Coulomb law. It is well known that the electrostatic field is modified because of the relativistic Lorentz contraction along the direction of motion, as shown in Fig. (I.12.1).

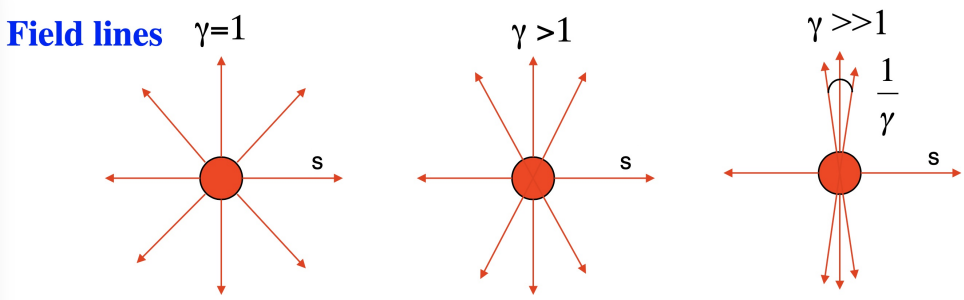

Fig. I.12.1: Electric field lines of a point charge at different energies.

For an ultra-relativistic charge, with $\gamma \gg 1$ the field lines are confined on a plane perpendicular to the direction of motion. In fact, if we suppose that the particle at $t = 0$ passes in the origin of the laboratory system, the electric field in the Cartesian coordinates can be written as

$$\mathbf{E} = \frac{q}{4\pi\varepsilon_0} \frac{\gamma \left(x\hat{i} + y\hat{j} + s\hat{k} \right)}{(x^2 + y^2 + \gamma^2 s^2)^{3/2}}. \tag{I.12.2}$$

At any point of the transverse plane perpendicular to the charge, since $z = 0$, if we write $x\hat{i} + y\hat{j} = r\hat{r}$, we have

$$\mathbf{E} = \frac{\gamma q}{4\pi\varepsilon_0 r^2} \hat{r}, \tag{I.12.3}$$

while, on the z axis, that is with $x = y = 0$, then

$$\mathbf{E} = \frac{q}{4\pi\varepsilon_0 \gamma^2 s^2} \hat{k}. \tag{I.12.4}$$

We see that in the transverse plane, the electric field is radial and proportional to the charge energy γ, while in the longitudinal plane, it vanishes as the inverse of the square of the energy.

Additionally, we also obtain that the magnetic field has only an azimuthal component of the kind

$$B_\theta = \frac{v}{c^2} E_r, \tag{I.12.5}$$

with circular field lines shown in Fig. I.12.2.

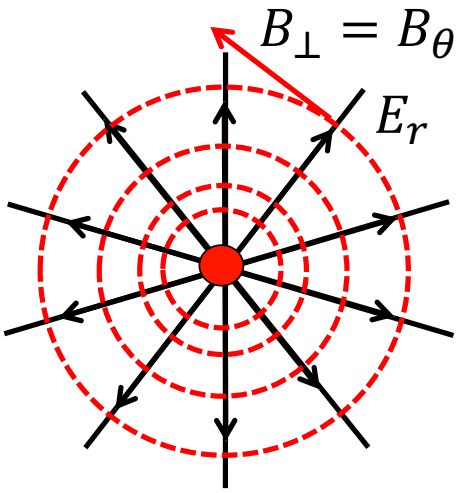

Fig. I.12.2: Electric and magnetic field lines of a relativistic point charge.

These fields allow evaluating the electromagnetic forces between two ultra-relativistic charges traveling with the same velocity on parallel trajectories at a distance r one from the other. In case the velocities are in the same direction, as in the left-hand side of Fig. I.12.3, the transverse force tends to vanish because electric and magnetic terms have opposite sign

$$F_r = q_1 \left(E_r - \beta c B_\theta\right) = \frac{\gamma q_1 q_2}{4\pi\varepsilon_0 r^2}\left(1-\beta^2\right) = \frac{q_1 q_2}{4\pi\varepsilon_0 \gamma r^2}. \tag{I.12.6}$$

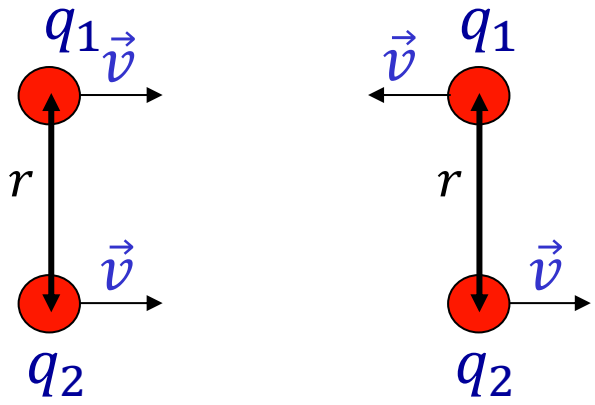

Fig. I.12.3: Two point charges moving in the same direction (left-hand side) and in the opposite direction (right-hand side).

This is generally the case for charges belonging to the same bunch ($q_1 = q_2$) giving rise to defocusing space charge effects, important for low-energy accelerators. On the other hand, if the two charges are moving in opposite directions, as in the right-hand side of the figure, the electric and magnetic forces have the same sign so that

$$F_r = q_1 \left(E_r + \beta c B_\theta\right) = \frac{\gamma q_1 q_2}{4\pi\varepsilon_0 r^2}\left(1+\beta^2\right). \tag{I.12.7}$$

Counter-rotating particles can be found, for example, during collisions, and they are important for beam-beam effects. In this case, the force can be defocusing or focusing if the two charges have the same or opposite sign.

We now analyze the case of a charge distribution. Let us consider an infinite uniform cylindrical beam of radius a in the free space. The intensity of the electric and magnetic fields can be computed like in the static case, applying Gauss's and Ampere's laws. Due to symmetries, the electric field is only radial and the magnetic field is azimuthal. As a consequence, it is convenient to choose, as the surface for the calculation of the electric field flux, a cylinder of radius r and length l symmetric to the beam. We observe that the flux is different from zero only on the lateral surface of the cylinder, where the electric field is constant. On the other hand, for the circulation of the magnetic field, we can choose a circumference of radius r. Referring to Fig. I.12.4, inside the distribution for $r \leq a$, we then have

$$2\pi r l E_r = \frac{\rho\pi r^2 l}{\varepsilon_0} = \frac{\lambda r^2 l}{a^2\varepsilon_0} \qquad \rightarrow \qquad E_r = \frac{\lambda r}{2\pi\varepsilon_0 a^2}, \tag{I.12.8}$$

$$2\pi r B_\theta = \mu_0 J \pi r^2 = \frac{\mu_0 v \lambda r^2}{a^2} \qquad \rightarrow \qquad B_\theta = \frac{\beta}{c}\frac{\lambda r}{2\pi\varepsilon_0 a^2}, \tag{I.12.9}$$

with ρ the volume charge density, λ the charge per unit of length and J the current density.

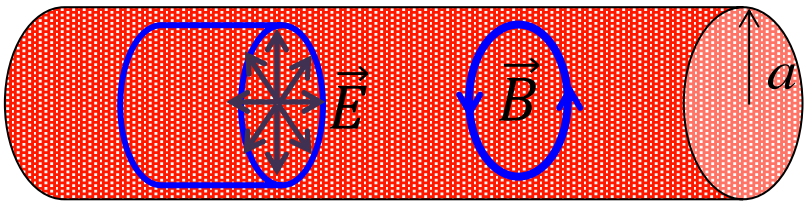

Fig. I.12.4: Infinite uniform cylindrical beam.

With these fields, the Lorentz force acting on a charge inside the distribution called direct space charge force is given by

$$F_r = q(E_r - v B_\theta) = q(1-\beta^2)E_r = \frac{qE_r}{\gamma^2} = \frac{q\lambda r}{2\pi\varepsilon_0\gamma^2 a^2}. \tag{I.12.10}$$

This force is positive, that is, defocusing, and it is linear with the transverse coordinate. The linearity derives from the assumption of uniform transverse distribution. We can observe that the attractive magnetic force, which becomes significant at high velocities, tends to compensate for the repulsive electric force so that the space charge defocusing is primarily a non-relativistic effect. Therefore, for very

high energy, these forces can be neglected.

Exercise 1

Calculate the electric and magnetic fields for $r \geq a$.

Exercise 2

Calculate the electric and magnetic fields in case of a transverse Gaussian distribution of the kind

$$\rho(r) = \frac{\lambda_0}{2\pi\sigma_r^2} e^{-\frac{r^2}{2\sigma_r^2}} \quad .$$

I.12.1.2 Indirect space charge forces

In an accelerator, the beams travel inside a vacuum pipe generally made of metallic material (aluminium, copper, stainless steel, etc.). The pipe goes through the coils of the magnets (dipoles, quadrupoles, sextupoles). Its cross-section may have a complicated shape, as in the case of special devices like RF cavity, kickers, diagnostics and controls; however, most part of the beam pipe has a cross-section with a simple shape: circular, elliptic, racetrack, or quasi-rectangular. For the moment we consider only the effect of a smooth pipe that influences the electromagnetic fields produced by the beam.

Before we go into this problem, it is necessary to recall the basic features of fields close to metallic or magnetic materials.

I.12.1.2.1 Boundary conditions

When we have two materials with different relative permittivity, which we call ε_{r1} and ε_{r2}, in the passage from one material to another, the tangential electric field and the normal electric displacement are preserved, so that we have the boundary relations

$$\begin{aligned} E_{t1} &= E_{t2} \\ \varepsilon_{r1} E_{n1} &= \varepsilon_{r2} E_{n2} \end{aligned} \quad . \tag{I.12.11}$$

If one of the two materials is a conductor with a finite conductivity and we are in the static condition, then the electric field must vanish inside it, and the walls are equipotential surfaces. This implies that the electric field lines are orthogonal to the conductor surface, independently of the dielectric and magnetic properties of the material. The only condition is to have a finite conductivity.

If we have a charge close to a conductor, in order to obtain the electric field, we need to include the effects of the induced charges on the conducting surfaces and we must know how they are distributed. Generally, this task is not easy, but if we have an infinite conducting screen, the problem can be easily solved by making use of the method of images: we can remove the screen and put, at a symmetric location, a "virtual" charge with opposite sign, as shown in the left-hand side of Fig. I.12.5, such that the potential is constant at the position of the screen and the field lines are orthogonal to its surface.

The total electric field outside of the conductor is the sum of that generated by the direct and the image charges.

For the static magnetic field between two materials with different permeability, the following

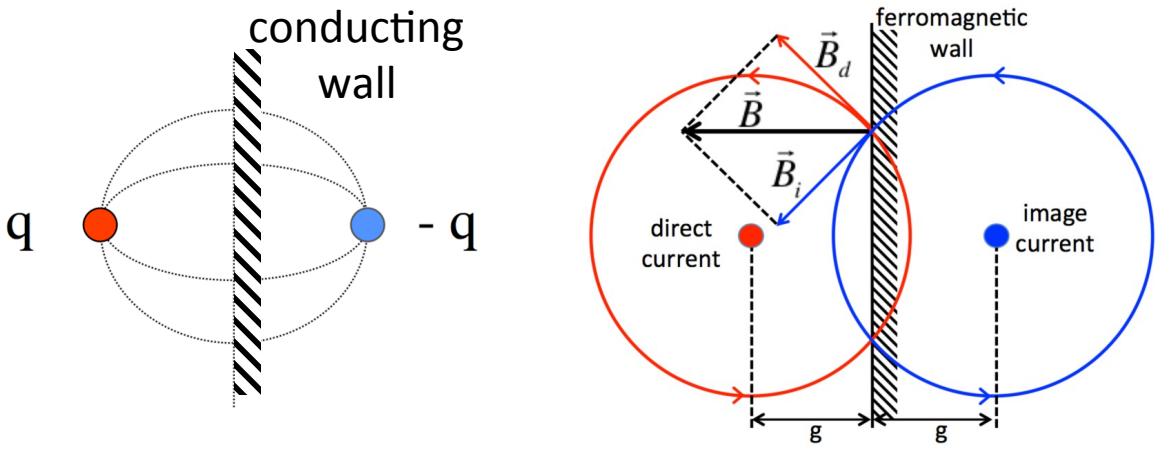

Fig. I.12.5: Left: image charge method for a charge near a conducting screen, right: image current method for a current near a ferromagnetic screen.

boundary relations hold

$$\begin{aligned} H_{t1} &= H_{t2} \\ \mu_{r1} H_{n1} &= \mu_{r2} H_{n2} \end{aligned} \quad . \tag{I.12.12}$$

Thus, static magnetic fields do not perceive the presence of the conductor, if it has a magnetic permeability $\mu_r \simeq 1$, as copper or aluminium, and the field lines behave as in the free space without any distortion. However, a beam pipe in a real machine goes through many magnetic components (like dipoles and quadrupoles) made of ferromagnetic materials with high permeability (of the order of $10^3 - 10^5$). For these materials, due to the boundary conditions, the magnetic field lines are practically orthogonal to the surface. Similarly to electric field lines for a conductor, the total magnetic field can be derived by using the image method: we remove the magnetic wall and put a symmetric current with the same sign, as shown on the right-hand side of Fig. I.12.5.

Static electric fields vanish inside a conductor for any finite conductivity σ, while static magnetic fields pass through, unless of high permeability. This is no longer true for time-changing fields, which can penetrate inside the material in a region δ_w called the skin depth. In order to obtain the skin depth as a function of the material properties, we use the following Maxwell's equations inside the conducting material together with the constitutive relations

$$\begin{cases} \nabla \times \mathbf{E} = -\dfrac{\partial \mathbf{B}}{\partial t} \\ \nabla \times \mathbf{H} = \mathbf{J} + \dfrac{\partial \mathbf{D}}{\partial t} \end{cases} \qquad \begin{cases} \mathbf{B} = \mu_0 \mu_r \mathbf{H} = \mu \mathbf{H} \\ \mathbf{D} = \varepsilon_r \varepsilon_0 \mathbf{E} = \varepsilon \mathbf{E} \\ \mathbf{J} = \sigma \mathbf{E} \end{cases} . \tag{I.12.13}$$

We suppose that both σ and μ do not depend on time. If we apply the curl to the first equation, we obtain

$$\nabla \times (\nabla \times \mathbf{E}) = \nabla (\nabla \cdot \mathbf{E}) - \nabla^2 \mathbf{E} = -\nabla^2 \mathbf{E} = -\frac{\partial}{\partial t} (\nabla \times \mathbf{B}) = -\mu \frac{\partial}{\partial t} (\nabla \times \mathbf{H}) . \tag{I.12.14}$$

We can substitute $\nabla \times \mathbf{H}$ with the second equation and use the constitutive relations so that the differential equation for the electric field becomes of the kind

$$\nabla^2 \mathbf{E} = \mu \frac{\partial \mathbf{J}}{\partial t} + \mu \frac{\partial^2 \mathbf{D}}{\partial t^2} = \mu\sigma \frac{\partial \mathbf{E}}{\partial t} + \mu\varepsilon \frac{\partial^2 \mathbf{E}}{\partial t^2}. \tag{I.12.15}$$

Consider a plane wave linearly polarized with the electric field in the x direction propagating in the conducting material along s. Then the differential equation becomes

$$\frac{\partial^2 E_x}{\partial s^2} - \mu\varepsilon \frac{\partial^2 E_x}{\partial t^2} - \mu\sigma \frac{\partial E_x}{\partial t} = 0. \tag{I.12.16}$$

A similar equation holds for H_y. With respect to the classic plane wave differential equation in vacuum, we now have an additional term proportional to the conductivity σ. In order to find the solution to this wave equation, we assume that the electric field propagates in the z direction according to

$$E_x = \tilde{E}_0 e^{j(\omega t - ks)}, \tag{I.12.17}$$

where $k = k_r + jk_i$ is a complex quantity that, from the above equation, is a solution of

$$-k^2 - j\omega\mu\sigma + \mu\varepsilon\omega^2 = 0, \tag{I.12.18}$$

that is

$$k = \pm\sqrt{\omega^2\mu\varepsilon\left(1 - \frac{j\sigma}{\omega\varepsilon}\right)}. \tag{I.12.19}$$

If $\sigma \gg \omega\varepsilon$, then we are in a good conductor condition and can write

$$k = k_r + jk_i \simeq \sqrt{\frac{\omega\sigma\mu}{2}} - j\sqrt{\frac{\omega\sigma\mu}{2}}. \tag{I.12.20}$$

Due to the imaginary part, the electric field propagates inside the conductor with an amplitude that attenuates exponentially inside the material according to

$$E_x = \tilde{E}_0 e^{-s/\delta_w} e^{j(\omega t - k_r s)}, \tag{I.12.21}$$

with the attenuation constant δ_w, having the units of meters, called skin depth and defined as

$$\delta_w = -\frac{1}{k_i} = \sqrt{\frac{2}{\omega\sigma\mu}}. \tag{I.12.22}$$

The skin depth depends on the material properties and the frequency. Copper, for example, has a skin depth of

$$\delta_w \simeq \frac{6.66}{\sqrt{f[\mathrm{Hz}]}}[\mathrm{cm}]. \tag{I.12.23}$$

If we assume a copper beam pipe 2 mm thick, for example, we find that fields pass through the wall up to frequencies of about 1 kHz.

These results allow us to obtain further boundary conditions when we have a time-varying e.m. field close to a good conductor with a given conductivity σ. In particular, if the skin depth is larger than the wall thickness, time-varying fields pass through the conductor wall. This happens at relatively low frequencies when δ_w is large. On the other hand, at higher frequencies, the skin depth can be much smaller than the wall thickness. In this case, we can consider that both electric and magnetic fields vanish inside the wall. As for the static case, we have that the electric field lines are perpendicular to the wall surface, while the magnetic field lines are tangent to the wall. As a consequence, in order to obtain a time-varying electric field close to a good conductor, we can still use the method of the images, while for the magnetic field, it is easy to see that we can use the method shown in Fig. I.12.6, by changing the direction of the image current.

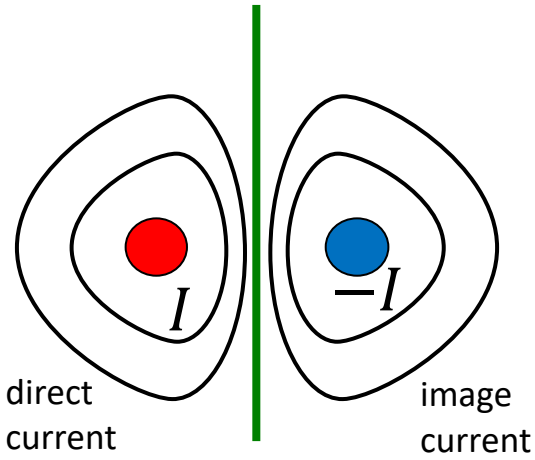

Fig. I.12.6: Image current method for a current near a ferromagnetic screen in case of a high-frequency magnetic field.

Exercise 3

Evaluate the electromagnetic force acting on a charge q at a distance d from an infinite perfectly conducting plane, moving with a relativistic velocity v parallel to the plane (see Fig. I.12.7).

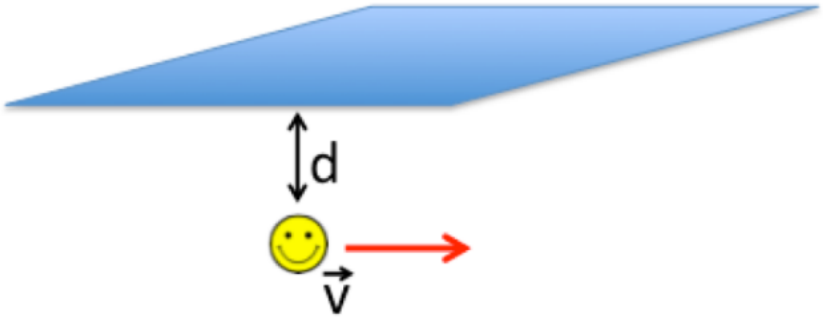

Fig. I.12.7: Exercise 3.

I.12.1.2.2 Indirect space charge forces of a beam in a circular beam pipe.

In the previous Section we have seen that, under certain conditions, the electric and magnetic fields of a charge or a distribution can be computed as the sum of the direct and image ones. As a first example of the application of this method, let us consider the case of an infinite uniform cylindrical beam, already studied in the free space, now placed in a circular beam pipe.

The direct force acting on any charge inside the distribution is given by Eq. (I.12.10). For the indirect force, we need to evaluate the fields due to the boundary conditions. In this case, however, due to the symmetry, the field lines are not modified by the presence of the vacuum chamber. Indeed, the electric field is already radial and then perpendicular to the pipe, and the magnetic field remains circular. Therefore, the transverse fields are the same as in the free space.

I.12.1.2.3 Space charge force for a finite length bunch

In the ultra-relativistic regime, with $\gamma \gg 1$, the same Eq. (I.12.10) can be used in the transverse plane even if the longitudinal distribution is not constant. For example, for bunched beams with finite length ℓ_0 inside a circular pipe of radius b, if $\ell_0 \gg b/\gamma$, by introducing the local charge density $\lambda(s)$ such that

$$\int_{\ell_0} \lambda(s) ds = Nq, \tag{I.12.24}$$

with N the total number of particles in the bunch and q the charge of a single particle, we can write the space charge force acting on a single particle inside the distribution as

$$F_r(s) = \frac{q\lambda(s)}{2\pi\varepsilon_0\gamma^2 a^2} r. \tag{I.12.25}$$

Exercise 4

By looking at Eq. (I.12.25), write the transverse electric and magnetic fields inside a cylindrical bunched ultra-relativistic beam in a circular vacuum chamber.

Exercise 5

Evaluate the total transverse space charge force (direct + indirect) acting on a charge inside an ultra-relativistic beam in a circular vacuum chamber for the following three longitudinal distributions:

- Gaussian: $\lambda(s) = \frac{Nq}{\sqrt{2\pi}\sigma_s} e^{-\frac{s^2}{2\sigma_s^2}}$;
- Parabolic: $\lambda(s) = \frac{3Nq}{2l_0}\left[1 - \left(\frac{2s}{l_0}\right)^2\right]$;
- Sinusoidal modulation: $\lambda(s) = \lambda_0 + \Delta\lambda\cos(k_s s)$.

I.12.1.2.4 Indirect space charge forces of a beam inside parallel plates: DC case

Under some conditions, the beam pipe cross-section is such that we can consider only the surfaces closer to the beam, which we can imagine as two parallel conducting plates, as shown in Fig. I.12.8 In this case, we can apply the image method to a charge distribution of radius a between two conducting plates $2h$ apart. For each plate, we have an image charge with an opposite sign with respect to the real charge at a

distance of $2h$. Each image charge, in its turn, must have a corresponding image charge with respect to the other plate so that we finally have an infinite set of charges with opposite signs $2h$ apart from each other as shown in Fig. I.12.9. In the figure, the charge distribution extends along the z axis.

Fig. I.12.8: Elliptic and rectangular vacuum chamber cross-section approximated by parallel plates.

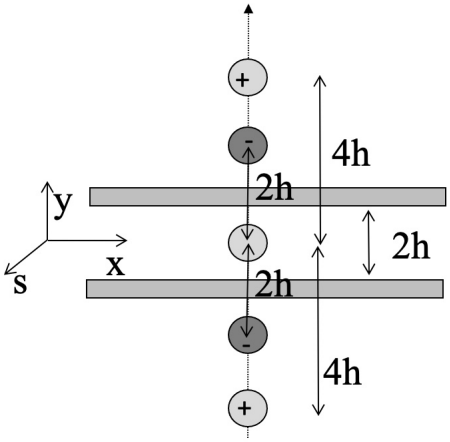

Fig. I.12.9: Image charge distribution for parallel plates.

By applying the superposition principle we get the total image electric field in a position y inside the beam as

$$E_y^{\text{im}}(y,s) = \frac{\lambda(s)}{2\pi\varepsilon_0}\sum_{n=1}^{\infty}(-1)^n\left(\frac{1}{2nh+y}-\frac{1}{2nh-y}\right) = \frac{\lambda(s)}{2\pi\varepsilon_0}\sum_{n=1}^{\infty}(-1)^n\frac{-2y}{(2nh)^2-y^2}$$
$$\simeq -\frac{\lambda(s)}{4\pi\varepsilon_0 h^2}y\sum_{n=1}^{\infty}(-1)^n\frac{1}{n^2} = \frac{\lambda(s)}{4\pi\varepsilon_0 h^2}\frac{\pi^2}{12}y. \quad \text{(I.12.26)}$$

In the last two passages, we have supposed that $h \gg a \geq y$. This expression represents the electric field due to the image charge distribution in a position y inside the circular beam. For the magnetic field, we can observe that it is not modified by the presence of the conducting plates so that the total vertical force acting on a charge inside the distribution, as a sum of the direct and indirect forces, is

$$F_y(y,s) = \frac{q\lambda(s)}{2\pi\varepsilon_0}\left(\frac{1}{\gamma^2 a^2}+\frac{\pi^2}{24h^2}\right)y. \quad \text{(I.12.27)}$$

In the above equation, the direct field is still given by Eq. (I.12.25) with r substituted here by y. Another interesting feature of this expression is that it is linear with the transverse coordinate y as long

as we remain inside the beam distribution, that is $y \leq a$. The linearity comes from the fact that we have supposed a transverse uniform distribution. Finally, observe that the $1/\gamma^2$ dependence is only valid for the direct space charge force since for image one there's no cancellation of the electric and magnetic forces.

Since we have lost the cylindrical symmetry due to the parallel plates, we need also to evaluate the horizontal space charge force. The direct force is the same as the vertical one since the beam has a cylindrical transverse distribution, while, for the image electric field we can use the divergence equation

$$\nabla \cdot \mathbf{E}^{\text{im}} = 0 \qquad (x, y) \leq a \tag{I.12.28}$$

so that

$$\frac{\partial E_x^{\text{im}}}{\partial x} = -\frac{\partial E_y^{\text{im}}}{\partial y} \rightarrow E_x^{\text{im}} = -\frac{\partial E_y^{\text{im}}}{\partial y} x = -\frac{\lambda(s)}{4\pi\varepsilon_0 h^2} \frac{\pi^2}{12} x. \tag{I.12.29}$$

As a consequence, the horizontal space charge force is

$$F_x(x, s) = \frac{q\lambda(s)}{2\pi\varepsilon_0} \left(\frac{1}{\gamma^2 a^2} - \frac{\pi^2}{24h^2} \right) x. \tag{I.12.30}$$

Observe that the presence of the parallel plates produces an image-defocusing force in the vertical plane and an image-focusing force in the horizontal plane.

Exercise 6

In the static case, evaluate the horizontal and vertical magnetic fields acting on a charge inside a beam at the center of two parallel plates having a distance $2g$ between each other, and made of magnetic material with $\mu_r \gg 1$.

I.12.1.2.5 Indirect space charge forces of a beam inside parallel plates: AC case

We have seen that, close to a conductor, electromagnetic fields have different behaviours depending on the skin depth of the material. Usually, in particular for bunched beams, the frequency spectrum is quite rich in harmonics. It is convenient to decompose the current into a DC component, $\bar{I} = \bar{\lambda} v$, for which the skin depth is much larger than the wall thickness, and an AC component, $\tilde{I} = \tilde{\lambda} v$, for which the skin depth is much lower than the wall thickness. While the DC component of the magnetic field does not perceive the presence of the material, its AC component is obliged to be tangent at the wall. As a consequence, we have image currents with opposite directions, which behave as the charges in the DC case, producing an image magnetic field. Therefore, we have now both image electric field $\tilde{E}_x^{\text{im}}$ and $\tilde{E}_y^{\text{im}}$, having the same expressions of the previous case, and image magnetic fields of the kind

$$\tilde{B}_x^{\text{im}}(s, y) = -\frac{\beta}{c} \tilde{E}_y^{\text{im}} \qquad \tilde{B}_y^{\text{im}}(s, y) = \frac{\beta}{c} \tilde{E}_x^{\text{im}}. \tag{I.12.31}$$

In this case, there's a cancellation of the electric and magnetic forces, so that the total forces acting on a charge inside the distribution and due to the AC component of the current can be written as

$$\tilde{F}_x(s) = \frac{q\tilde{\lambda}(s)}{2\pi\varepsilon_0\gamma^2} \left(\frac{1}{a^2} - \frac{\pi^2}{24h^2} \right) x \tag{I.12.32}$$

$$\tilde{F}_y(s) = \frac{q\tilde{\lambda}(s)}{2\pi\varepsilon_0\gamma^2}\left(\frac{1}{a^2} + \frac{\pi^2}{24h^2}\right) y. \tag{I.12.33}$$

A similar method can be applied when the beam is inside two parallel plates made of ferromagnetic material, as, for example, when outside the beam pipe there is a dipole magnet with half-gap g. For the DC case, the magnetic field doesn't see the conducting pipe, while it is strongly affected by ferromagnetic material, and the field lines must be orthogonal to the pole surface so that the total magnetic field can be obtained by considering image currents with the same sign.

It is possible to write an expression that summarizes the results under the different conditions (AC or DC) on both axes as

$$F_u = \frac{q}{\pi\varepsilon_0}\left[\frac{1}{\gamma^2}\left(\frac{1}{2a^2} \mp \frac{\pi^2}{48h^2}\right)\lambda \mp \beta^2\left(\frac{\pi^2}{48h^2} + \frac{\pi^2}{24g^2}\right)\bar{\lambda}\right] u, \tag{I.12.34}$$

where $\bar{\lambda}$ is the DC part of the current. The upper (minus) sign is used when $u = x$, while the lower (plus) sign is used when $u = y$. It is interesting to observe that these forces are linear with transverse displacement $u = x$ or y. This is due to the hypothesis of uniform transverse distribution. A more general expression, valid also for geometries different from circular or parallel plates, can be written as

$$F_u = \frac{q}{\pi\varepsilon_0}\left[\frac{1}{\gamma^2}\left(\frac{f_0}{a^2} \mp \frac{f_1}{h^2}\right)\lambda \mp \beta^2\left(\frac{f_1}{h^2} + \frac{f_2}{g^2}\right)\bar{\lambda}\right] u. \tag{I.12.35}$$

The Laslett form factors f_0, f_1, and f_2 depend on the pipe geometry. By comparing the above equation with Eq. (I.12.34), for example, it is easy to obtain the coefficients for the parallel planes.

Exercise 7

Demonstrate Eq. (I.12.31) by starting from the magnetic field of an infinite straight wire and using the method of image currents.

Exercise 8

Write the Laslett form factors for parallel plates.

I.12.1.3 Longitudinal space charge force

In the longitudinal plane, the space charge force can be obtained, under some simplified assumptions, from the transverse fields. In particular, let us consider a cylindrical beam inside a cylindrical vacuum chamber of radius b at ultra-relativistic velocities so that, according to the discussion at the end of Sec. I.12.1.2.2, the results that we obtain for an infinite uniform cylindrical beam can be extended also to bunched beams. The geometry is shown in Fig. I.12.10.

Let us use Faraday's law of induction by choosing, as an integration path, a small rectangle with two sides parallel to the $s-$axis, one starting from inside the beam at a given distance r in a given longitudinal position z, and the parallel one going through the beam pipe at $r = b$ as in the figure. We can write

$$\oint \mathbf{E}\cdot\mathbf{dl} = -\frac{\partial}{\partial t}\int_S \mathbf{B}\cdot\mathbf{dS}. \tag{I.12.36}$$

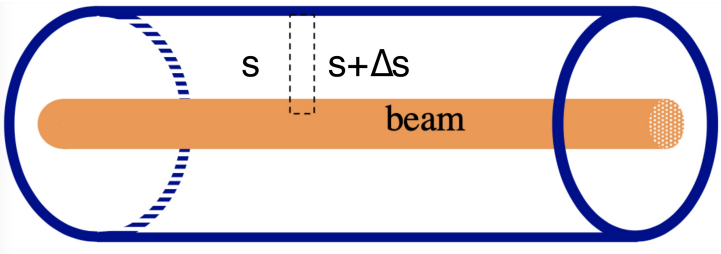

Fig. I.12.10: Beam model used to determine the longitudinal space charge forces.

Since Δs is an infinitesimal, the above integral equation can be expanded as

$$E_s(r,s)\Delta s + \int_r^b E_r(r',s+\Delta s)dr' - E_s(b,s)\Delta s - \int_r^b E_r(r',s)dr' = \\ -\Delta s \frac{\partial}{\partial t}\int_r^b B_\theta(r',s)dr'. \quad \text{(I.12.37)}$$

The difference between the two radial electric fields inside the integrals in the left-hand side of the above equation can be written as

$$E_r(r',s+\Delta s) - E_r(r',s) = \frac{\partial E_r(r',s)}{\partial s}\Delta s, \quad \text{(I.12.38)}$$

so that the equation becomes

$$E_s(r,s) = E_s(b,s) - \int_r^b \left[\frac{\partial E_r(r',s)}{\partial s} + \frac{\partial B_\theta(r',s)}{\partial t}\right] dr'. \quad \text{(I.12.39)}$$

We also observe that there is a relation between the longitudinal position s and time t: a charge arriving earlier in a given position of a circular machine with respect to the reference particle for which $s = 0$ has a negative time but positive s since it is ahead with respect to the reference particle. We have therefore $ds = -vdt$, with v the velocity of the beam, so that

$$E_s(r,s) = E_s(b,s) - \frac{\partial}{\partial s}\int_r^b \left[E_r(r',s) - vB_\theta(r',s)\right] dr'. \quad \text{(I.12.40)}$$

From Eq. (I.12.9), and noting that, for perfectly conducting walls, we have $E_s(b,s) = 0$, the longitudinal electric field inside the beam becomes

$$E_s(r,s) = -\frac{\partial}{\partial s}\int_r^b \left[E_r(r',s) - \beta^2 E_r(r',s)\right] dr' = -\frac{1}{\gamma^2}\frac{\partial}{\partial s}\int_r^b E_r(r',s)dr'. \quad \text{(I.12.41)}$$

The integral on the right-hand side of the equation depends on the beam distribution. If we consider a uniform cylindrical beam of radius a, then the integral can be split into an integral inside the beam (from r to a), for which the radial electric field is given by Eq. (I.12.8), and an integral from a to b, outside the

beam, for which the electric field is proportional to $1/r$, so that we obtain

$$E_s(r,s) = -\frac{1}{4\pi\varepsilon_0\gamma^2}\left(1 - \frac{r^2}{a^2} + 2\ln\frac{b}{a}\right)\frac{\partial\lambda(s)}{\partial s}. \tag{I.12.42}$$

Since the magnetic field does not affect the longitudinal force, we have

$$F_s(r,s) = qE_s(r,s) = -\frac{q}{4\pi\varepsilon_0\gamma^2}\left(1 - \frac{r^2}{a^2} + 2\ln\frac{b}{a}\right)\frac{\partial\lambda(s)}{\partial s}. \tag{I.12.43}$$

Observe that this force is proportional to the derivative of the longitudinal distribution with the minus sign: a positive slope means a negative force and vice versa. For a bunched beam, having, for example, Gaussian or parabolic line density distribution, positive slopes in $\lambda(s)$ are in the tail of the bunch where charges are then affected by a negative longitudinal force and lose energy. The opposite happens for charges in the head of the bunch, which are then accelerated. Of course, a uniform longitudinal distribution does not produce any longitudinal force due to symmetry conditions. Observe also that this force is inversely proportional to γ^2 and vanishes quickly in high-energy accelerators.

Exercise 9

Demonstrate Eq. (I.12.42) by solving the integral (I.12.41) with the proper expression of $E_r(r,s)$.

Exercise 10

Compute the longitudinal space charge forces produced by a cylindrical beam in a circular beam pipe with the same longitudinal distributions as Exercise 5.

Comments on Exercise 10 Let us suppose a coasting beam inside a circular accelerator working below the transition energy. The longitudinal space charge force is proportional to

$$-\frac{\partial\lambda(s)}{\partial s}.$$

As a consequence, particles along the positive slope of sinusoidal modulation are affected by a negative force and lose energy. The opposite happens to particles on the negative slope. Below transition energy particles with energy lower than the nominal one have a longer revolution time thus delaying a bit. This means that such particles tend to slide down the slopes of the sinusoidal modulation, thus filling the valleys of the perturbation which then decreases in amplitude as shown with the red curve of Fig. I.12.11. The perturbation tends to cancel out and the beam is stable. The opposite happens above transition energy, thus producing an increase of the perturbation: this is called a negative mass instability, and it is caused by the space charge above the transition energy.

I.12.1.4 Transverse incoherent space charge effects in circular accelerators

In order to study the effects of the transverse space charge forces on beam dynamics, we consider an ideal circular accelerator of radius ρ with the coordinate system already used in Chapters I.3 and I.4 on transverse and longitudinal beam dynamics. The equation of motion can be derived starting from Newton's second law. However, different from the equations used in the transverse beam dynamics, here we must take into account not only the external guiding forces but also the self-field ones produced by

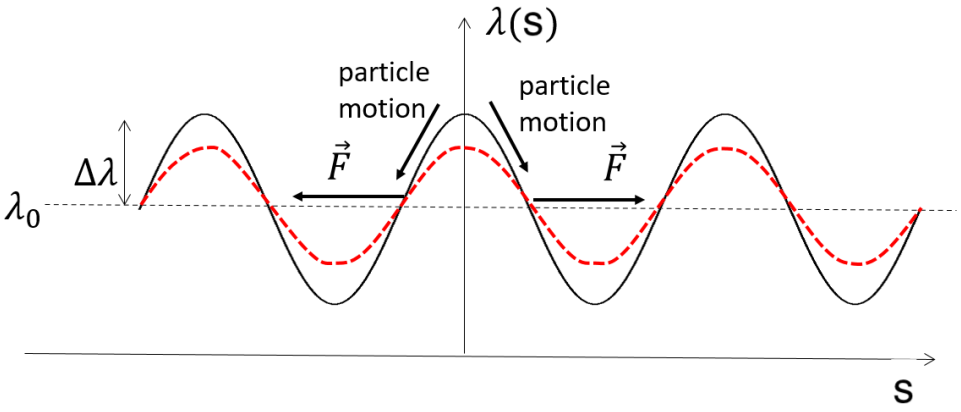

Fig. I.12.11: Effect of the longitudinal space charge force on a coasting beam below transition energy.

the space charge. Therefore, our starting equation is

$$\frac{d(\gamma m_0 \mathbf{v})}{dt} = \mathbf{F}^{\text{ext}}(\mathbf{r}) + \mathbf{F}^{\text{self}}(\mathbf{r}) \qquad \rightarrow \qquad \frac{d\mathbf{v}}{dt} = \frac{\mathbf{F}^{\text{ext}}(\mathbf{r}) + \mathbf{F}^{\text{self}}(\mathbf{r})}{\gamma m_0}, \tag{I.12.44}$$

for which we are supposed to have a constant beam energy since the external forces are produced by static magnetic fields. Starting from this equation, we follow the same procedure used to derive the linear betatron equation of motion (see Chapter I.3 on transverse deam dynamics), but we now must also take into account the transverse space charge forces in addition to the guiding and focusing forces of dipoles and quadrupoles. As a consequence, we can now write

$$x''(s)v^2 - \frac{v^2}{\rho}\left[1 - \frac{x(s)}{\rho}\right] = -\frac{qvB_0}{\gamma m_0} - \frac{qvxg}{\gamma m_0} + \frac{F_x^{\text{self}}}{\gamma m_0}. \tag{I.12.45}$$

By dividing both sides of this equation by v^2, we get

$$x''(s) + x(s)\left(\frac{1}{\rho^2} + k\right) = \frac{F_x^{\text{self}}}{\gamma v^2 m_0} = \frac{F_x^{\text{self}}}{\beta^2 E_0}, \tag{I.12.46}$$

with E_0 the beam energy. Since we want to study the perturbation to the betatron motion produced by the space charge forces, in the following we adopt the simplified model in which the particles execute simple harmonic oscillations around the reference orbit. This is the case for which the focusing term is constant along the machine. Although this condition is never fulfilled in a real accelerator, it provides a reliable model for the description of the effects due to the self-fields. As a consequence, we consider the focusing term between the round brackets on the left-hand side of the equation as a constant K_x, so that the differential equation of motion becomes

$$x''(s) + K_x x(s) = \frac{1}{\beta^2 E_0} F_x^{\text{self}}. \tag{I.12.47}$$

We want also to express the above equation in terms of the betatron tune Q_{x0}. For that, we write

the solution of the free betatron motion as

$$x(s) = A_x \cos\left(\sqrt{K_x}s + \psi\right), \tag{I.12.48}$$

from which we can define a betatron wavelength as

$$\lambda_\beta = \frac{2\pi}{\sqrt{K_x}}. \tag{I.12.49}$$

From this wavelength, we define the betatron tune as

$$Q_{x0} = \frac{2\pi\rho}{\lambda_\beta} = \rho\sqrt{K_x}, \tag{I.12.50}$$

so that the equation of motion becomes

$$x''(s) + \left(\frac{Q_{x0}}{\rho}\right)^2 x(s) = \frac{1}{\beta^2 E_0} F_x^{\text{self}}. \tag{I.12.51}$$

It is important to remember that in deriving this equation we have linearized the betatron motion on the left-hand side, but no assumptions have been made for the space charge force. Let us now consider an expansion of the self-forces around the ideal orbit: the constant term acts as a dipole magnet and changes the equilibrium orbit, and the linear term (proportional to the displacement) acts as a quadrupole changing the focusing strength and thus inducing a shift of the betatron frequencies. This can happen either in the motion of individual particles inside the beam (incoherent motion), or in the oscillation of the whole beam (coherent motion) around the closed orbit.

If we write the linear term of the space charge force as

$$\left(\frac{\partial F_x^{\text{self}}}{\partial x}\right)_0 x, \tag{I.12.52}$$

then the equation becomes

$$x''(s) + \left[\left(\frac{Q_{x0}}{\rho}\right)^2 - \frac{1}{\beta^2 E_0}\left(\frac{\partial F_x^{\text{self}}}{\partial x}\right)_0\right] x(s) = 0. \tag{I.12.53}$$

We recognize in the square brackets a term proportional to the square of the new betatron tune that is shifted, with respect to the initial one Q_{x0} by the self-induced forces. This term can then be written as

$$\left[\left(\frac{Q_{x0}}{\rho}\right)^2 - \frac{1}{\beta^2 E_0}\left(\frac{\partial F_x^{\text{self}}}{\partial x}\right)_0\right] = \frac{(Q_{x0} + \Delta Q_x)^2}{\rho^2} \simeq \frac{Q_{x0}^2 + 2Q_{x0}\Delta Q_x}{\rho^2}, \tag{I.12.54}$$

for which we have supposed that the perturbation to the tune ΔQ_x (the tune shift) is much smaller than the unperturbed tune, that is $\Delta Q_x \ll Q_{x0}$.

By comparing the first and the last term of the above equation, we obtain the tune shift due to the

space charge forces as

$$\Delta Q_x = -\frac{\rho^2}{2\beta^2 E_0 Q_{x0}} \left(\frac{\partial F_x^{\text{self}}}{\partial x} \right)_0 . \tag{I.12.55}$$

Depending on the case, F_x^{self} can be any of the expressions derived in Secs. I.12.1.1 and I.12.1.2. For the vertical plane or in the case of cylindrical symmetry, we can substitute x with y or r respectively. For the case of direct space charge force and in a circular vacuum chamber, the betatron tune shift is negative since the space charge forces are defocusing on both planes. Notice also that, since the transverse self-force for a non-uniform longitudinal distribution depends on the longitudinal position inside the beam, the tune shift is not constant along the beam: charges at different positions are affected by different space charge forces thus giving a tune spread inside the beam. This conclusion is generally true also for more realistic non-uniform transverse beam distributions, which are characterized by a tune shift dependent also on the betatron oscillation amplitude. In these cases, the effect is called incoherent tune spread. The term incoherent derives from the fact that the tune shift changes for different charges inside the bunch. In addition to this, there can be another effect acting on the center of mass of a bunch called coherent tune shift, as we will discuss in the next Section.

As an example, let us consider an ultra-relativistic bunch with uniform circular transverse distribution on the axis of a circular pipe. The space charge force is given by Eq. (I.12.25), so that the tune shift can be written as

$$\Delta Q_x = -\frac{q\rho^2}{4\pi\varepsilon_0\gamma^2\beta^2 a^2 E_0 Q_{x0}}\lambda(s) = -\frac{r_{e,p}\rho^2}{q\gamma^3\beta^2 a^2 Q_{x0}}\lambda(s), \tag{I.12.56}$$

where $r_{e,p}$ is the classical radius of the electron or the proton and $q = 1.6 \times 10^{-19}$ C the electron charge. In this expression, we can clearly see the dependence of the tune shift on the longitudinal position inside a beam.

Exercise 11

Calculate the tune spread (which we can simply define here as the difference between the minimum and maximum tune shifts of the charges inside the distribution) for the three distributions of Exercise 5.

Some effects of the longitudinal distribution on the tune spread are discussed in the Appendix I.12.A.

In the more general and realistic case of non-uniform focusing along the accelerator, we can get back to Eq. (I.12.47) considering K_x as a function of s and, as done for the constant focusing, linearize the space charge force so that, instead of Eq. (I.12.53) we obtain

$$x''(s) + \left[K_x(s) - \frac{1}{\beta^2 E_0} \left(\frac{\partial F_x^{\text{self}}(s)}{\partial x} \right)_0 \right] x(s) = x''(s) + \left[K_x(s) + \Delta K_x(s) \right] x(s) = 0. \tag{I.12.57}$$

Observe that we have considered here that also F_x^{self} can vary along the machine.

This equation clearly shows that the space charge forces act as a gradient error $\Delta K_x(s)$ located at a given position s of the machine. From the beam optics it is possible to demonstrate that, having a circular accelerator with design quadrupole strength $K_x(s)$ and gradient errors $\Delta K_x(s)$ distributed along

the machine, these errors lead to a tune shift of

$$\Delta Q_x = \frac{1}{4\pi}\oint \beta_x(s)\Delta K_x(s)ds = -\frac{1}{4\pi\beta^2 E_0}\oint \beta_x(s)\left(\frac{\partial F_x^{\text{self}}(s)}{\partial x}\right)_0 ds, \tag{I.12.58}$$

where β_x is the betatron function. With this expression, we can remove the hypothesis of a constant focusing along the machine.

Exercise 12

Consider a beam with uniform circular transverse distribution inside a circular vacuum chamber of constant radius a. Express the betatron tune shift of Eq. (I.12.56) in terms of the beam emittance.

Exercise 13

Evaluate Eq. (I.12.58) for a uniform transverse distribution of radius a using the relation $a^2 = \beta_x\varepsilon_x$ with ε_x the horizontal beam emittance.

Why can a space charge tune shift be dangerous? Since each particle inside the bunch can have a different tune shift, the final result of the transverse space charge forces is a spread of the betatron tunes. However, in circular accelerators, the values of the betatron tunes should not be close to rational numbers in order to avoid the crossing of linear and non-linear resonances where the beam becomes unstable. The spread induced by the space charge force can make it hard to satisfy this basic requirement. Typically, in order to avoid major resonances, the stability requires that [1]

$$\Delta Q_{x/y} \leq 0.5. \tag{I.12.59}$$

If the tune spread exceeds this limit, it could be necessary to reduce the effects of space charge tune spread, e.g. by increasing the injection energy or the transverse beam size.

Exercise 14

To reduce the effects of the space charge tune spread, one possible action is to increase the beam injection energy. In the CERN Proton Synchrotron (PS), for example, the last upgrade program increased the injection (kinetic) energy from 1.4 GeV to 2 GeV. Determine the relative reduction in the tune spread. The proton rest energy is 0.938 GeV.

The incoherent tune spread discussed so far also produces a beneficial effect, called Landau damping (see Appendix I.12.D.1), which, under some conditions, can cure different beam instabilities.

I.12.1.5 Coherent tune shift: uniform beam off-axis in a circular pipe

When a bunch is off-axis, for example, because of an injection error or a transverse deflection kick, it starts to perform betatron oscillations as a whole, as shown in Fig. I.12.12. The bunch, which is the source of the space charge fields, moves transversely inside the pipe, but the direct space charge forces in its center of mass (CM in the figure) must be zero due to symmetry. However, image space charge can affect bunch motion.

Let us consider an infinite circular beam with uniform line density λ_0 displaced by a distance x off-axis with respect to the center of a cylindrical vacuum chamber of radius b, as shown in Fig. I.12.13. We have already studied that the electric field lines of the beam must be perpendicular to the pipe walls.

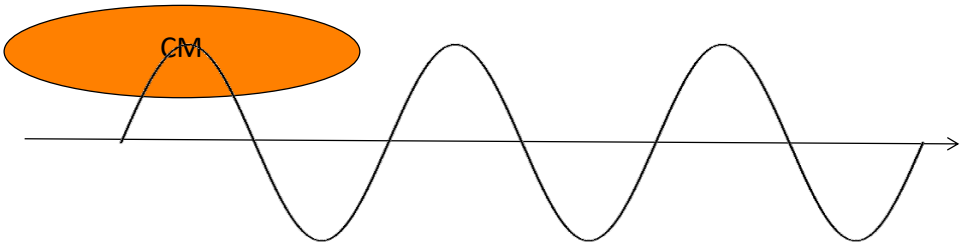

Fig. I.12.12: Coherent betatron oscillations.

It can be demonstrated that such a configuration of the field lines can be obtained by using an image charge distribution $-\lambda_0$ at a distance $d = b^2/x$ from the pipe centre (see demonstration in Appendix I.12.B). With such a configuration, the walls of the vacuum chamber are equipotential.

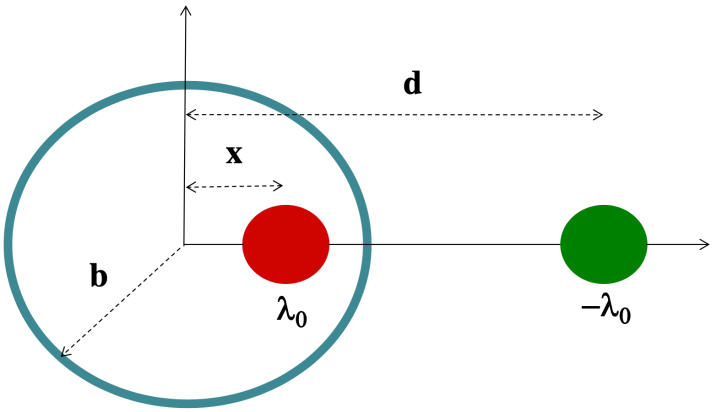

Fig. I.12.13: Geometry used in the coherent tune shift evaluation.

In the centre of mass of the beam, the direct space charge forces are zero, but the image charge distribution produces an electric field equal to[1]

$$E_{x,\text{coh}} = \frac{\lambda_0}{2\pi\varepsilon_0}\frac{1}{d-x} \simeq \frac{\lambda_0}{2\pi\varepsilon_0}\frac{1}{d} = \frac{\lambda_0}{2\pi\varepsilon_0}\frac{x}{b^2}, \tag{I.12.60}$$

for which we have supposed $x \ll d$. This linear electric field produces an attractive force on the centre of the beam in the positive direction of the x-axis of the kind

$$F_{x,\text{coh}} = \frac{q\lambda_0}{2\pi\varepsilon_0}\frac{x}{b^2}. \tag{I.12.61}$$

Being the force linear with x, we can apply the same method that we have used for the incoherent tune shift and obtain the coherent tune shift due to the image space charge of a uniform beam off-axis in

[1] Observe that the electric field expression is proportional to $1/r$ as that of an infinite linear wire.

a circular beam pipe as

$$\Delta Q_{x,\text{coh}} = -\frac{\rho^2}{2\beta^2 E_0 Q_{x0}} \left(\frac{\partial F^{\text{self}}_{x,\text{coh}}}{\partial x} \right)_0 = -\frac{\rho^2}{2\beta^2 E_0 Q_{x0}} \frac{q\lambda_0}{2\pi\varepsilon_0 b^2}. \tag{I.12.62}$$

I.12.1.6 Longitudinal space charge effects in circular accelerators

In the longitudinal plane we can follow a reasoning similar to the transverse case and obtain the synchrotron equation of motion with the inclusion of the longitudinal space charge forces F_s^{self} as

$$\Delta\phi'' + \left(\frac{Q_s}{\rho} \right)^2 \Delta\phi = \frac{h\eta}{\rho\beta^2 E_0} F_s^{\text{self}}, \tag{I.12.63}$$

where $\Delta\phi$ is the relative RF phase with respect to the synchronous particle, h is the harmonic number, η is the slippage factor, and Q_s is the synchrotron tune, defined as the ratio between the synchrotron angular frequency ω_s and the revolution angular frequency ω_0, and given by

$$Q_s = \frac{\omega_s}{\omega_0} = \sqrt{\frac{q\eta h V_{\text{RF}} \cos\phi_s}{2\pi\beta^2 E_0}}, \tag{I.12.64}$$

with V_{RF} the RF peak voltage, and ϕ_s the synchronous phase. If the longitudinal space charge forces can be linearized, the effect is a shift of the synchrotron tune as in the transverse plane.

Another important consideration about the longitudinal plane is that since the force acts in the same direction as the motion of the charges, it changes their energy. This can have consequences on the longitudinal beam distribution depending if the machine operates below or above transition energy.

I.12.2 Wakefields

In addition to space charge, self-induced electromagnetic forces can also be generated by the beam interacting with the different devices distributed along the accelerator, or due to the finite conductivity of the vacuum chamber. These devices may have a complex geometry: kickers, bellows, RF cavities, diagnostics components, collimators, and other special devices. The study of these fields requires solving the Maxwell equations in a given structure taking the beam current as source. This is a quite complicated task for which it has been necessary to develop dedicated computer codes, which solve the electromagnetic problem in the frequency or in the time domain. There are several useful codes developed for the electromagnetic design of accelerator devices such as CST Studio Suite, GDFIDL, ACE3P, ABCI, and others.

In this Section, we first discuss the general features of these fields, introduce the concept of wakefield (or wake function) and coupling impedance, and then show a few simple examples in cylindrical geometry: the finite conductivity of a circular beam pipe and the resonant modes of an RF cavity. In addition, although the space charge forces have been studied previously, under some conditions, they can also be considered as a particular case of wakefields.

I.12.2.1 Definition of wakefields

Let us consider two charges inside a bunch, q_0 and q called source and test charge, respectively, moving at the speed of light along parallel trajectories inside a generic structure, as represented in Fig. I.12.14.

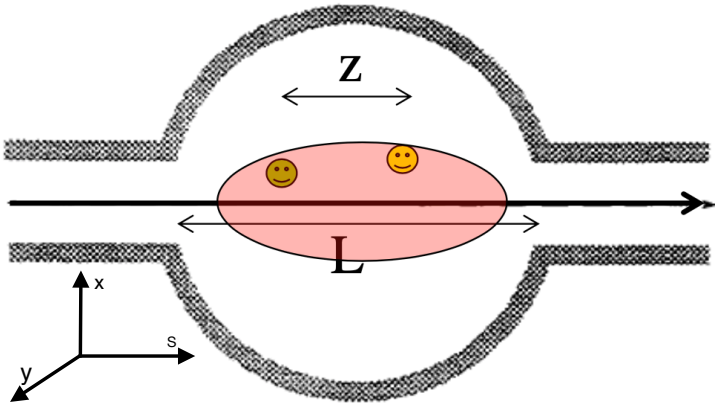

Fig. I.12.14: Geometry used for the definition of wakefields.

Let $\mathbf{E}$ and $\mathbf{B}$ be the fields generated by q_0 inside the structure, $(s_0 = ct, r_0)$ be the position of the source charge and $(s = s_0 + z, r)$ be the position of the test charge q. If $z > 0$ then the test particle is ahead of the source. Since the velocity of both charges is along the z-axis, the Lorentz force acting on q has the following components [2]

$$\mathbf{F} = q\left[E_s\hat{k} - (E_x - cB_y)\,\hat{\imath} + (E_y + cB_x)\,\hat{\jmath}\right] = \mathbf{F}_{\parallel} + \mathbf{F}_{\perp}. \tag{I.12.65}$$

It is convenient to distinguish two effects on the test charge: the longitudinal force changes the particle energy, while the transverse force deflects its trajectory. Additionally, we use two approximations valid for high energy accelerators [3, 4]:

- The rigid beam approximation, which says that the beam moves rigidly through the structure and the electromagnetic field is a perturbation that does not affect its motion during the passage. This implies that the distance z between the two charges and their transverse positions do not change inside the structure;
- The impulse approximation: although the test charge sees a force coming from the electromagnetic field all along the structure, what it cares about is the impulse variation through the entire device

$$\Delta\mathbf{p} = \int_{\text{structure}} \mathbf{F}dt. \tag{I.12.66}$$

Under these two hypotheses, we are not interested in the force acting on the test charge point by point inside the structure, but in the integral of the force along the charge trajectory. The effect of the longitudinal component of this force is then an energy change

$$U(r, r_0, z) = v\Delta p_s = \int_{\text{structure}} F_{\parallel} ds \simeq U(z). \tag{I.12.67}$$

This energy change, which represents the work done by the force, is expressed in Joule. It is positive if the test charge gains energy, and negative if it loses it. In obtaining this expression we are also supposed to be in cylindrical symmetry so that it is possible to expand $U(r, r_0, z)$ in the transverse coordinates and take only the first term of the expansion $U(z)$ independent on both r and r_0.

If we consider the transverse force, we obtain a transverse deflecting kick

$$\mathbf{M}(r, r_0, z) = v\Delta\mathbf{p}_\perp = \int_{\text{structure}} \mathbf{F}_\perp ds \simeq r_0 \mathbf{M}(z). \tag{I.12.68}$$

The unit here is (N·m), and, as for the longitudinal plane, we are supposed to be in cylindrical symmetry by keeping only the first-order term expansion in the transverse coordinates which is, in this case, proportional to the transverse position of the source charge. This is also called “dipolar term", and it is a vector since it can be different in the two planes x and y. For devices which do not have a cylindrical symmetry, in the expansion, it is also important to consider the term proportional to the transverse displacement of the test charge r (called quadrupolar or detuning term).

The above two quantities $U(z)$ and $\mathbf{M}(z)$, normalized by the two charges, are called longitudinal and transverse dipolar wakefields[2], given respectively by

$$w_\parallel(z) = \frac{U(z)}{qq_0}, \tag{I.12.69}$$

$$\mathbf{w}_\perp(z) = \frac{\mathbf{M}(z)}{qq_0}. \tag{I.12.70}$$

Units are V/C and V/C/m. The longitudinal wakefield then represents the energy lost or gained by a test charge following the source one at a distance z in passing through a structure and due to the electromagnetic fields of the source. In some textbooks, it is defined with the minus sign, so that a positive sign of the wakefield means lost energy. In the transverse plane, a positive wakefield means a defocusing deflecting force.

The wakefields are independent of the properties of the charges and depend only on the geometry and conductivity of the device. A wakefield can be considered as the Green function of the device.

I.12.2.2 Loss factor and beam-loading theorem

The loss factor represents the energy lost by a charge in passing through a structure due to the electromagnetic fields of the charge itself and normalized by q_0^2. It is therefore defined as

$$k_\parallel = \frac{U(z=0)}{q_0^2}. \tag{I.12.71}$$

Although in general the loss factor is given by the longitudinal wakefield at $z = 0$, for charges travelling with the speed of light, $w_\parallel(z = 0)$ is discontinuous at $z = 0$ due to the causality principle, as shown in Fig. I.12.15, where an example of the longitudinal wake function is shown when $\beta = 1$. Indeed

[2] They are also called wake functions.

the exact relationship between the loss factor and the wakefield is given by the beam-loading theorem

$$k_{\parallel} = \frac{w_{\parallel}(z \to 0^{-})}{2}. \tag{I.12.72}$$

This relation is only true in the longitudinal plane.

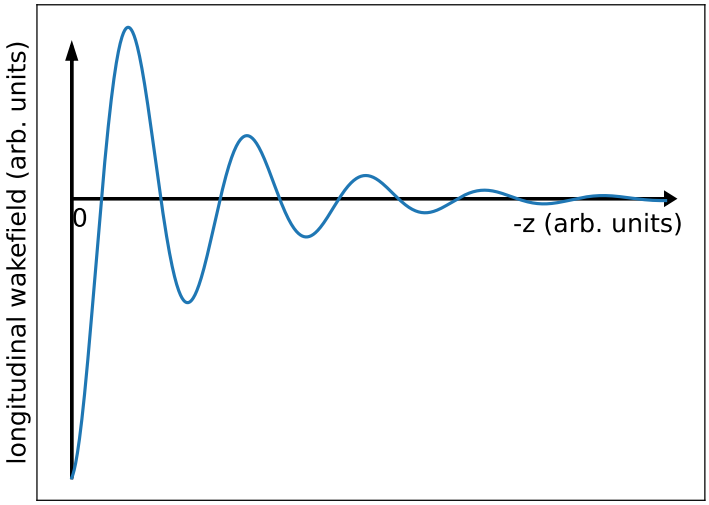

Fig. I.12.15: Example of wakefield with $\beta = 1$.

For a simple demonstration of the beam-loading theorem, let us consider a charge q moving at the speed of light that is split into two charges of value $q/2$ at a distance z one from the other. Let us call A the head charge and B the tail one. The energy lost by A can be only due to the loss factor because of the causality principle. We can then write

$$U_A = q_A^2 k_{\parallel} = \frac{q^2}{4} k_{\parallel}, \tag{I.12.73}$$

with $k_{\parallel}$ the loss factor. For the charge B the energy loss is due to the electromagnetic field of the charge itself, that is $k_{\parallel}$ plus that due to the wake produced by A, that is

$$U_B(z) = q_B^2 k_{\parallel} + q_B q_A w_{\parallel}(z) = \frac{q^2}{4} k_{\parallel} + \frac{q^2}{4} w_{\parallel}(z). \tag{I.12.74}$$

When $z \to 0$ the sum $U_A + U_B$ must be equal to the loss factor of the original charge q, so that

$$q^2 k_{\parallel} = U_A + U_B(z \to 0^{-}) = \frac{q^2}{2} k_{\parallel} + \frac{q^2}{4} w_{\parallel}(z \to 0^{-}), \tag{I.12.75}$$

from which we obtain Eq. (I.12.72).

I.12.2.3 Wake potential and energy loss of a bunched distribution

Another quantity of interest related to the wakefield in the longitudinal plane is the amount of energy a particle gains or loses due to the electromagnetic fields produced by the same bunch it belongs to. Let us suppose to have a longitudinal distribution $\lambda(s) = dq/ds$, with

$$q_{\text{tot}} = \int_{-\infty}^{\infty} \lambda(s) ds \tag{I.12.76}$$

the total bunch charge, and a particle of charge q in a position s inside this distribution, as represented in Fig. I.12.16.

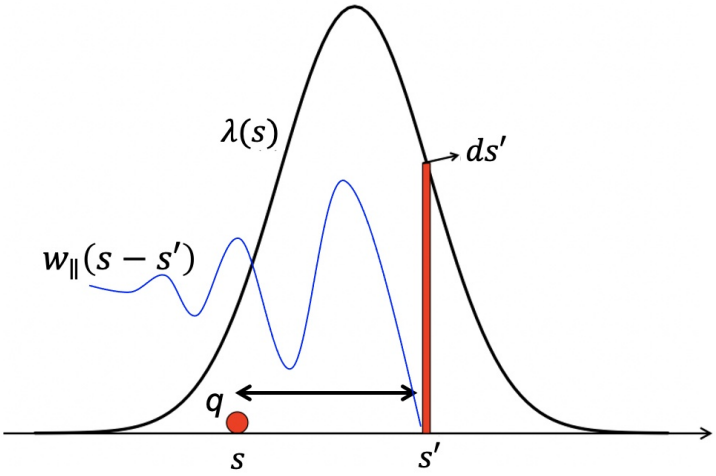

Fig. I.12.16: Model for the evaluation of the longitudinal wake potential.

By using the definition of wakefield given by Eq. (I.12.69), we can write the energy change of q due to all the charges $dq(s')$ that are in a position s' inside the longitudinal distribution as

$$dU(s) = qdq(s')w_{\parallel}(s - s') = qw_{\parallel}(s - s')\lambda(s')ds'. \tag{I.12.77}$$

By using the superposition principle we can sum this elementary energy change over the whole bunch, obtaining the energy variation of the charge q as

$$U(s) = q \int_{-\infty}^{\infty} w_{\parallel}(s - s')\lambda(s')ds'. \tag{I.12.78}$$

If the bunch is travelling at the speed of light, due to the causality principle, we know that the wake is zero ahead of the source, so that all the charges behind e cannot contribute to its energy change and the above equation can also be written as

$$U(s) = q \int_{s}^{\infty} w_{\parallel}(s - s')\lambda(s')ds'. \tag{I.12.79}$$

This energy change allows us to define the wake potential as the convolution integral of the wake-

field and the longitudinal distribution normalized by the bunch charge, that is

$$W_{\parallel}(s) = \frac{U(s)}{qq_{\text{tot}}} = \frac{1}{q_{\text{tot}}} \int_{-\infty}^{\infty} w_{\parallel}(s - s')\lambda(s')ds'. \tag{I.12.80}$$

Also in the transverse plane, of course, it is possible to define a wake potential similar to the longitudinal case. In this case, it is proportional to the transverse momentum, and it represents a normalized transverse deflecting kick of a charge due to the entire bunch.

Knowing the longitudinal wake potential, it is easy to evaluate the energy variation of the entire bunch due to the electromagnetic field of the bunch itself. Indeed, if we divide $U(s)$ by the point charge e and multiply it by all the charges in s, that is, $\lambda(s)ds$, we obtain the energy change of this infinitesimal slice. By summing over all the slices, we get

$$U_{\text{bunch}} = \frac{1}{q} \int_{-\infty}^{\infty} U(s)\lambda(s)ds = q_{\text{tot}} \int_{-\infty}^{\infty} W_{\parallel}(s)\lambda(s)ds. \tag{I.12.81}$$

I.12.2.4 Coupling impedance

In several cases, it is convenient to solve the Maxwell equations and evaluate the electromagnetic fields not in the time domain but in the frequency domain. In these conditions, we do not directly obtain the wakefield, but its Fourier transform. Additionally, the analytical approach normally used to study collective effects in circular accelerators consists of transforming in the frequency domain the differential equation describing the motion of the whole beam, which, under some very common conditions, is called the Vlasov equation. This implies that the wakefields also need to be transformed.

The Fourier transforms of the longitudinal and transverse wakefields are therefore just as important quantities as the wakes themselves. They are called coupling impedances since their unit is ohm and are defined as

$$Z_{\parallel}(\omega) = -\frac{1}{c} \int_{-\infty}^{\infty} w_{\parallel}(z)e^{-i\omega z/c}dz, \tag{I.12.82}$$

$$\mathbf{Z}_{\perp}(\omega) = \frac{i}{c} \int_{-\infty}^{\infty} \mathbf{w}_{\perp}(z)e^{-i\omega z/c}dz. \tag{I.12.83}$$

The imaginary term i was introduced in the definition of the transverse coupling impedance to make the transverse impedance have the same role as the longitudinal one in the study of collective effects. If the charge does not travel at the speed of light, instead of c in the two equations, we must substitute the velocity of the charge v. With the negative sign in front of Eq. (I.12.82), a positive real part of the impedance is related to lost energy. This notation is followed by important electromagnetic codes listed in the following Section and used to determine the wake potentials and the coupling impedances of the machine devices.

I.12.2.5 Comments on wakefield, wake potential and electromagnetic codes

The difference between the wakefield, which represents the energy lost by a test particle in passing through a device due to the electromagnetic field of a source particle and normalized by the two charges, and the wake potential, representing the energy lost by the test charge due to the electromagnetic field of

the whole bunch, again normalized by the charges, deserves here some additional comments.

First of all, we must say that the study of the electromagnetic fields inside an accelerator device requires solving the Maxwell equations by taking the beam current as the source of the fields and considering the walls of the structure as boundary conditions. This is quite a complicated task. Indeed, only for a few simple geometries it is possible to solve analytically the electromagnetic problem, but, for more realistic devices it has been necessary to develop dedicated computer codes, which solve the Maxwell equations in the time or in the frequency domain. In the last case, as a result, we obtain the coupling impedances.

There are several codes that are used for the electromagnetic design of accelerator devices, and new ones are being developed. Without intending to be exhausting, we mention here some of them:

- CST Microwave Studio: Computer Simulation Technology (https://www.cst.com);
- GDFIDL: Gitter drüber, fertig ist die Laube, literally: a simple way to build an arbour, is by putting up a mesh (http://www.gdfidl.de);
- ACE3P: Advanced Computational Electromagnetic 3D Parallel software (https://confluence.slac.stanford.edu/display/AdvComp/ACE3P+-+Advanced+Computational+Electromagnetic+Simulation+Suite);
- ECHO(2D, 3D): Electromagnetic Code for Handling Of Harmful Collective Effects (https://echo4d.de/echo2d/);
- ABCI: Azimuthal Beam Cavity Interaction (https://abci.kek.jp/).

All these codes work in the time domain and provide, as a result, the wake potential of a given longitudinal distribution, and not the wakefield. With the inverse Fourier transform and by dividing the result by the bunch spectrum, they also give the coupling impedance up to a maximum frequency that depends on the chosen distribution.

According to Eq. (I.12.80), if we know the wakefield (Green function) of a given device, we can obtain the wake potential for any distribution, but the contrary is not possible: the wake potential is valid only for a fixed distribution.

As a consequence, for beam dynamics studies, we should know the wake potential for any possible distribution that the beam could assume. In a Linac, with particles moving at the speed of light, the longitudinal distribution remains frozen in time, and a fixed wake potential can be used to evaluate the energy variation of particles inside the bunch (energy spread), while a fixed transverse wake potential can be used to evaluate the deflecting kick. In this situation, the knowledge of a single wake potential can be sufficient to study the beam dynamics.

On the other hand, in a circular accelerator, the longitudinal position of a charge depends on its energy through the slippage factor, and this energy is modified by the wake potential. As a consequence, the wake potential changes the longitudinal distribution, which, in turn, changes the wake potential. In this case, we have to study the beam dynamics in a self-consistent way. Knowledge of the wake potential of a given distribution is not sufficient because we do not know what the equilibrium beam distribution will be due to the wake and other solutions have to be found. For example, in many cases, the wake potential of a very short bunch can be used as an approximate wakefield to reconstruct the wake potential

of longer bunches.

I.12.2.6 Resistive wall

An example of a wakefield that can be obtained analytically is represented by the case of a cylindrical vacuum chamber of length ℓ and radius b with high conductivity σ_c such that the skin depth is much smaller than the thickness of the wall (the so-called thick wall regime). Additionally, we consider $\beta = 1$ and a frequency range such that

$$\frac{c\xi}{b} \ll \omega \ll \frac{c\xi^{-1/3}}{b}, \tag{I.12.84}$$

with

$$\xi = \frac{1}{Z_0 \sigma_c b} \tag{I.12.85}$$

with Z_0 the vacuum impedance. Under such conditions, it is possible to solve the Maxwell equations in cylindrical coordinates using the beam as a source [3]. We do not write here explicitly the calculations, but the longitudinal coupling impedance results to be

$$Z_{\parallel} = (1-i)\frac{\ell}{2\pi b}\sqrt{\frac{Z_0\omega}{2c\sigma_c}} = \frac{\ell}{2\pi b}(1-i)\frac{1}{\delta_w \sigma_c} = \frac{\ell}{2\pi b} Z_{\text{surf}}, \tag{I.12.86}$$

where we have separated the dependence on geometry from the dependence on material properties (skin depth and conductivity). The quantity Z_{surf} is called surface impedance.

An analogous expression can be written in the transverse plane, where we have an impedance that is inversely proportional to the third power of the pipe radius.

In order to better understand the frequency range in which this impedance is valid, suppose that we have an aluminium beam pipe ($\sigma_c = 3.5 \times 10^7$ S/m) with a radius of 5 cm. From Eq. (I.12.84), we obtain that

$$1.4 \ll f \ll 8.3 \times 10^{11} \tag{I.12.87}$$

with f the frequency in Hz. As you can see, this is a very large interval of validity.

From the impedance, with the inverse Fourier transform, it is also possible to obtain the longitudinal wakefield, equal to

$$w_{\parallel}(z) = -\frac{\ell c}{4\pi b}\sqrt{\frac{Z_0}{\pi\sigma_c}}\frac{1}{|z|^{3/2}}. \tag{I.12.88}$$

Also, this wakefield has an interval of validity. Indeed $|z|$ must satisfy the condition

$$\xi^{1/3} b \ll |z| \ll \frac{b}{\xi}. \tag{I.12.89}$$

With the same above example, the range of validity for the wakefield is

$$57\mu\text{m} \ll |z| \ll 3.3 \times 10^7 \text{m}. \tag{I.12.90}$$

As for the impedance, there's also an expression for the transverse resistive wall wakefield under the same conditions. This wake is inversely proportional to the third power of the pipe radius and to

$1/\sqrt{|z|}$.

The longitudinal resistive wall impedance has also a quite simple physical interpretation. Referring to Fig. I.12.17 where we have represented a model of the cylindrical beam pipe of radius b and length ℓ, we can imagine that, while the beam is passing, there is a flow of induced current inside the pipe walls, which moves along ℓ and remains confined within the skin depth δ_w. The section through which the image current flows is then a circular ring that, if $b \gg \delta_w$, is equal to

$$S \simeq 2\pi b \delta_w. \tag{I.12.91}$$

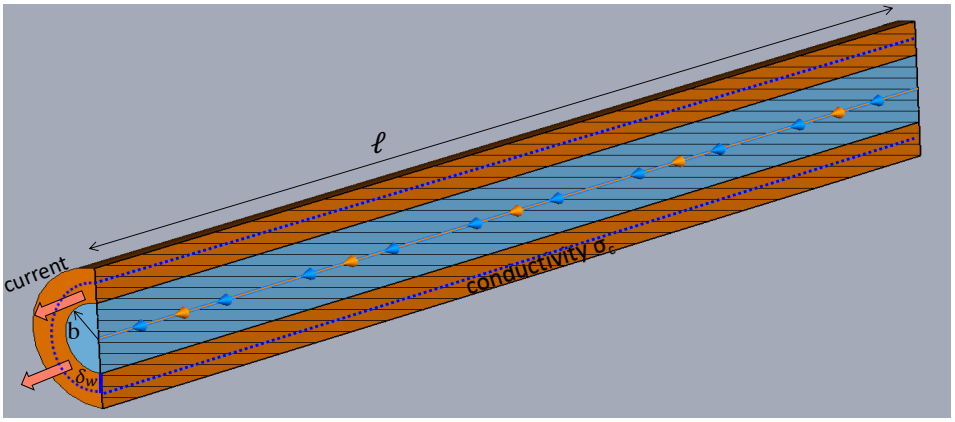

Fig. I.12.17: Model of beam pipe for the interpretation of the real part of the resistive wall impedance.

This induced current moves inside the conductor and it encounters a resistance equal to

$$R = \frac{\ell}{\sigma_c S} = \frac{\ell}{2\pi b}\frac{1}{\sigma_c \delta_w}. \tag{I.12.92}$$

Therefore, this resistance is exactly the real part of the longitudinal coupling impedance of Eq. (I.12.86) that can be interpreted as the resistance encountered by the induced current flowing inside the walls of the beam pipe, in a thickness equal to the skin depth.

For the interpretation of the imaginary part, we can use the following argument which refers to Fig. I.12.18. We have already seen that the induced current flows through an area of section $S = 2\pi b\delta_w$. This area is represented in blue and is zoomed in on the right-hand side of the figure. If we call the induced current I, we can also define a current density

$$J = \frac{I}{S} = \frac{I}{2\pi b \delta_w}. \tag{I.12.93}$$

This current produces a magnetic field inside S with circular concentric field lines. If we consider a circumference of radius r as that shown in the right-hand side of the figure ($r \simeq b$), we can write Ampere's law as

$$2\pi r B \simeq 2\pi b B = \mu J 2\pi b(r-b), \tag{I.12.94}$$

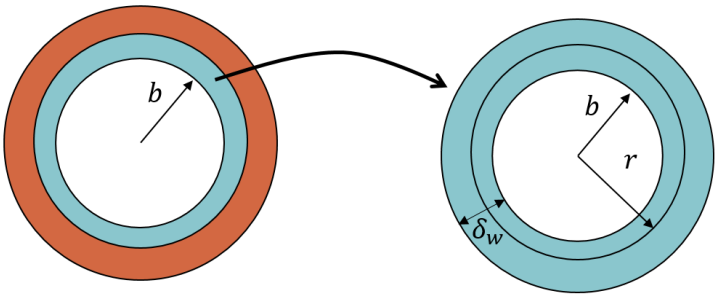

Fig. I.12.18: Model of beam pipe for the interpretation of the imaginary part of the resistive wall impedance.

so that

$$B = \mu J(r - b) \tag{I.12.95}$$

in the first-order approximation.

The flux of B through a surface of length ℓ and width δ_w is then

$$\Phi(B) = \ell\mu J \int_b^{b+\delta_w} (r - b)dr = \frac{\ell\mu J}{2}\delta_w^2 = \frac{\ell\mu I\delta_w}{4\pi b}, \tag{I.12.96}$$

where, for the last passage, we have used Eq. (I.12.93).

Having obtained the flux of the magnetic field, we can define an inductance as the ratio of the flux and the current so that

$$L = \frac{\Phi}{I} = \frac{\ell\mu\delta_w}{4\pi b}. \tag{I.12.97}$$

The imaginary part of the impedance is then equal to

$$Z_{\text{im}}(\omega) = -\omega L = -\frac{\ell}{2\pi b}\frac{\omega\mu\delta_w}{2} = -\frac{\ell}{2\pi b}\sqrt{\frac{2\mu^2\omega^2}{4\omega\sigma_c\mu}} = -\frac{\ell}{2\pi b}\sqrt{\frac{Z_0\omega}{2c\sigma_c}}, \tag{I.12.98}$$

which coincides with the imaginary term of the longitudinal coupling impedance of Eq. (I.12.86).

An example of low-frequency resistive wall impedance is shown in Fig. I.12.19, where we have compared Eq. (I.12.86) with the results of the CST Microwave Studio electromagnetic code.

For the comparison of the wakefield, as we have already discussed, we cannot directly use the results of CST because the code can only give the wake potential of a given distribution. However, if we use Eq. (I.12.88) and do the convolution integral defined in Eq. (I.12.80) with a Gaussian longitudinal distribution, we obtain the wake potential shown, with the green curve, in Fig. I.12.20 where we have also represented the result of CST (simulations). The two curves agree very well.

I.12.2.7 Space charge

As a second example of evaluation of impedance and wakefield, let us consider the longitudinal space charge force that we have obtained in Section I.12.1.3. Actually, space-charge effects are a bit on the edge of the definition of wakefields. Indeed, the definitions of eqs. (I.12.69) and (I.12.70) give a wake

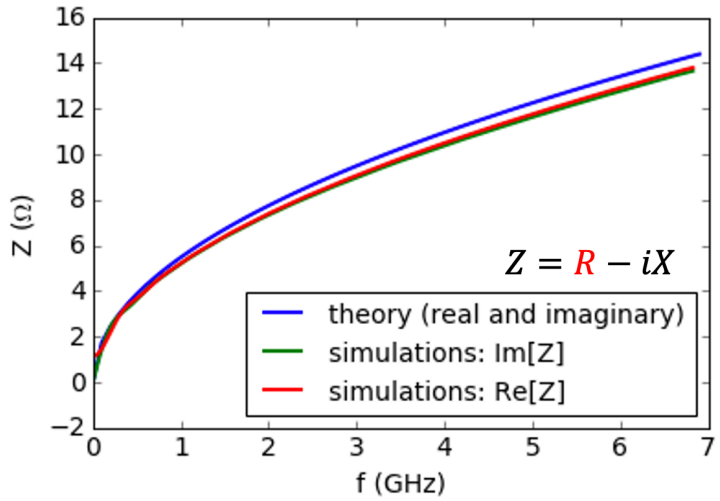

Fig. I.12.19: Classical thick-wall impedance as a function of frequency. Comparison between analytical expression and the CST Microwave Studio results.

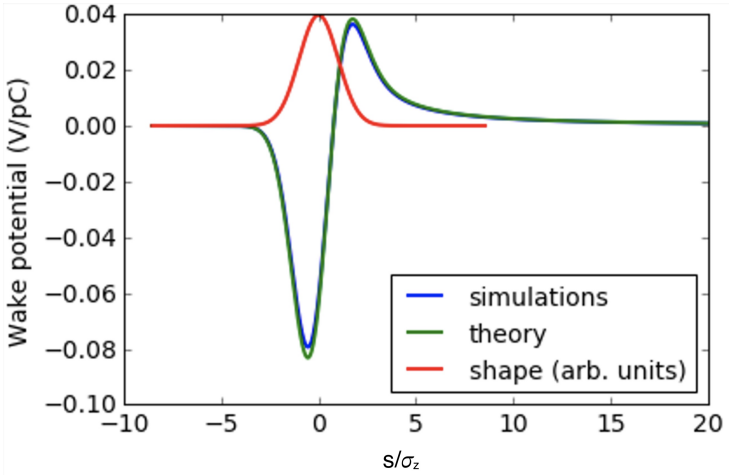

Fig. I.12.20: Resistive wall wake potential of a Gaussian bunch.

dependent on the geometry of the device, but independent on the properties of the charges, while we have seen that space charge forces depend, for example, on the bunch energy and distribution. However, we can still define a wakefield with space charge forces by considering a moderately relativistic beam with $\gamma \gg 1$ but not infinite. It turns out that in such a condition, starting from the force given by, for example, by Eq. (I.12.43), we can still define a wakefield, even if it depends on beam properties such as the transverse beam radius a and the beam energy γ. Let us consider a relativistic beam with cylindrical symmetry and uniform transverse distribution inside a circular pipe so that the longitudinal space charge force is given by Eq. (I.12.43). We can assume that the test particle is on axis ($r = 0$) and that the source is a point charge, so that, in terms of the longitudinal distribution, this source is proportional to the Dirac delta function: $\lambda(s) = q_0\delta(s)$. Since this longitudinal force is constant in the beam pipe where we want

to evaluate the space charge, from Eqs. (I.12.67) and (I.12.69), we obtain that

$$w_{\parallel}(z) = \frac{1}{qq_0}\int_0^{\ell} F_s(0,z)ds = -\frac{\ell}{4\pi\varepsilon_0\gamma^2}\left(1+2\ln\frac{b}{a}\right)\delta'(z), \tag{I.12.99}$$

where ℓ is the length of the structure (beam pipe) and δ' is the derivative of the Dirac delta function. With this wake and the definition of coupling impedance given by Eq. (I.12.82), by supposing, in this case of space charge, that the particle velocity is not exactly c but $v = \beta c$, we have

$$Z_{\parallel}(\omega) = \frac{\ell}{4\pi\varepsilon_0 v\gamma^2}\left(1+2\ln\frac{b}{a}\right)\int_{-\infty}^{\infty}\delta'(z)e^{-i\omega z/v}dz = i\frac{\ell\omega Z_0}{4\pi c\beta^2\gamma^2}\left(1+2\ln\frac{b}{a}\right). \tag{I.12.100}$$

Observe that this impedance is purely imaginary and is linearly proportional to the frequency. However, unlike a pure inductive impedance, such as, for example, that given by Eq. (I.12.98), this one has the opposite sign.

Exercise 15

Evaluate the energy lost per unit length by a charge inside a given longitudinal distribution $\lambda(z)$ due to the longitudinal wakefield of the space charge and compare it with the longitudinal space charge force in $r = 0$.

Exercise 16

From the result of the previous exercise, evaluate the total energy lost per unit length by the whole bunch.

Exercise 17

Evaluate the energy spread ($U_{\text{max}} - U_{\text{min}}$) of a Gaussian bunch of RMS length σ due to the longitudinal wakefield of the space charge in a structure of length ℓ.

I.12.2.8 Wakefield and coupling impedance of a whole accelerator

In the previous Sections, we have discussed two examples of wakefield and impedances, due to resistive wall and the space charge. Similar studies, also with the help of electromagnetic codes, must be performed for other accelerator devices, such as RF systems, collimation systems, bellows, and so on. Once we have the results for all or at least the main ones, the total machine impedance (and wakefield) can be obtained by summing all the elements.

In this way, we consider the contribution of each element independent of the presence of the others, that is, we ignore any possible interference effects between different devices.

An example of the wake and coupling impedance of a whole machine is represented in Fig. I.12.21 for the DAΦNE accumulator ring [5]. On top of the figure, the wake potential is represented. We recall that only with a few simplified models it is possible to obtain the analytical wakefield of a point charge, that is, the Green function. For realistic structures, we need to resort to the simulation codes that provide the wake potential of a given distribution. In this case, a Gaussian bunch of 5 mm rms has been used. The total bunch length for this machine has been measured to be about 4 cm, which is a factor of about 10 larger so that this wake can be used as a pseudo-Green function. The corresponding coupling impedance, obtained with the Fourier transform of the wake potential divided by the Gaussian bunch spectrum, is shown in the lower part of the figure. Actually, instead of $Z_{\parallel}(\omega)$, here we have represented $Z_{\parallel}(\omega)/n$

with $n = \omega/\omega_0$ and ω_0 the angular revolution frequency. This quantity is generally used for evaluating longitudinal instabilities

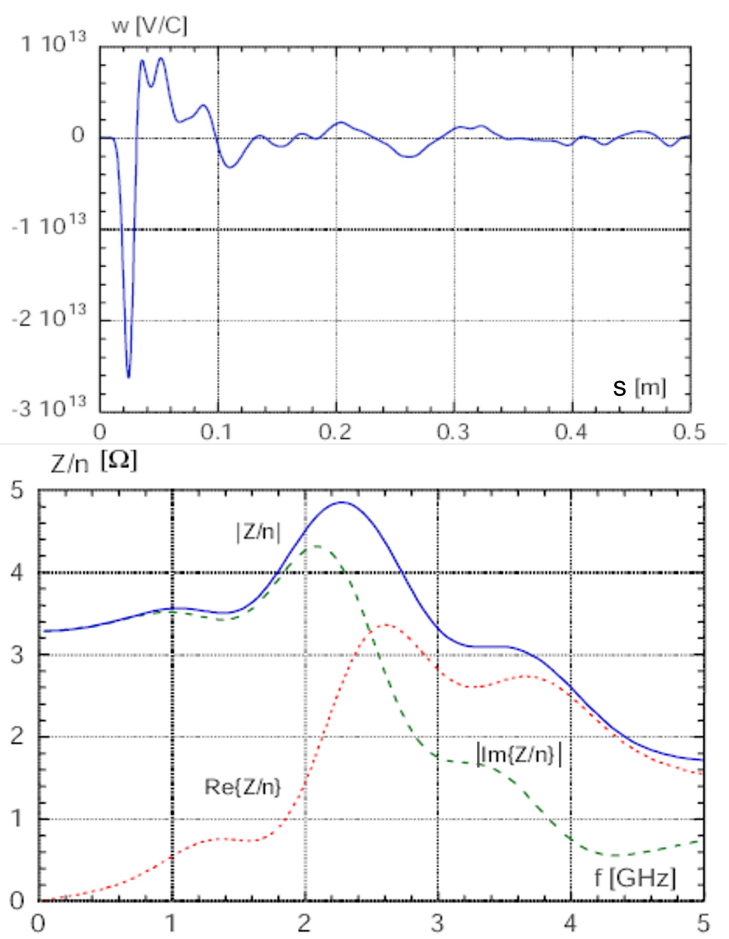

Fig. I.12.21: Example of wake potential (top) and coupling impedance (bottom) of the DAΦNE accumulator ring [5].

I.12.2.9 Short and long-range wakefield

In the previous Section, we have shown an example of the so-called short-range wakefield (wake potential in this case). Another example is represented in Fig.I.12.22 for the DAΦNE main ring [6]. In this case, also the bunch shape used to determine the wake potential is shown. This figure allows us to highlight the characteristic of the short-range wake: it vanishes after a few bunch lengths so that at the passage of another bunch or the same one after one machine turn, the wake is zero and, consequently, only the single bunch beam dynamics is influenced.

Concerning the coupling impedance, we know that the frequency resolution of the Fourier transform depends on the total time of the signal. Due to the fact that this wake goes rapidly to zero, we have a poor frequency resolution. The frequency transform is therefore called the broadband impedance. Even if the true impedance of a machine can have very complicated behaviour, with many peaks as a function of frequency, the broadband impedance, as shown in the bottom part of Fig. I.12.21, does not contain

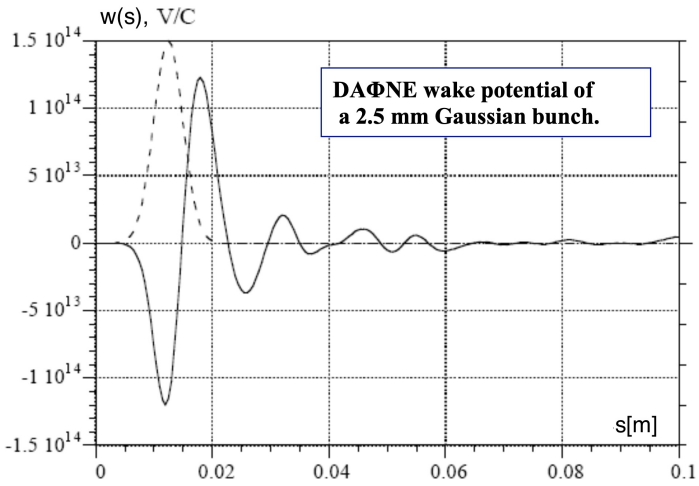

Fig. I.12.22: Short range wake potential of the DAΦNE main ring [6].

such details that, on the other hand, are not necessary for single-bunch dynamics studies.

In addition to the broadband impedance, a bunch can also excite resonant modes when it passes through a machine device. These resonant modes are produced by electromagnetic fields which keep on oscillating inside a structure after the bunch has left it. Eventually, the same bunch, or others, can interact with these fields when they enter the structure. In this case, we call them long-range wakefields. They are characterized by fields that oscillate over long distances. Therefore, they influence the multi-bunch (or multi-turn) beam dynamics. In the frequency domain, they are characterized by a high peak real part of the impedance. This impedance can be described by only three parameters: the quality factor of the mode, Q, its resonant frequency f_r, and the peak value of its real part, called shunt resistance R_s.

An example of a long-range wakefield produced by a point charge is shown in Fig. I.12.23 together with a given longitudinal bunch distribution (Gaussian in this case). As we can see from the figure, after the bunch passage, the wake is still strong so that it can influence a second bunch which enters after a given time interval in the same structure. Eventually, this second bunch can also excite the same wake which can, then, increase its amplitude.

The corresponding coupling impedance, real and imaginary, is represented in Fig I.12.24 with the narrow peak clearly shown.

A typical impedance like this can be found in resonant structures, such as the RF cavity. For this device, a charge can excite not only the fundamental, accelerating mode but other several resonant modes, also called High Order Modes (HOMs). It is possible to demonstrate that, under some conditions, each mode can be treated as an electric RLC parallel circuit loaded by an impulsive current. A qualitative explanation of this behaviour can be given with the help of Figs. I.12.25.

On the left-hand side of the figure, a pillbox cavity is shown when a point charge q_0 (here supposed negative) enters it. The two vertical plates of the structure, except from the holes necessary for the connection with the beam vacuum chamber, can be seen as two parallel plates of a capacitor. When the negative charge is close to one of the plates, it induces a positive charge on it, as shown in the figure. Due

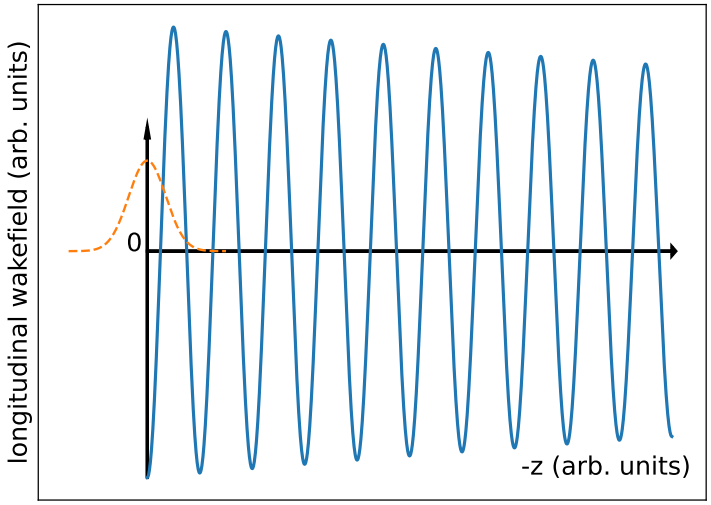

Fig. I.12.23: Example of long range wake field.

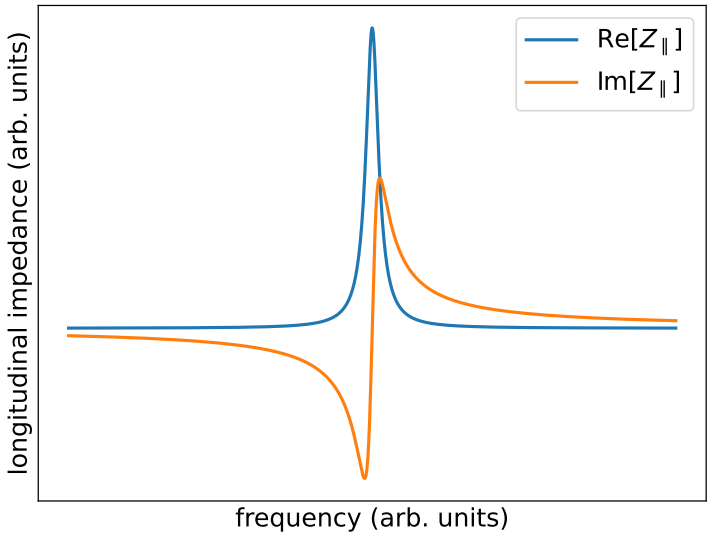

Fig. I.12.24: Example of narrow peak impedance produced by a high-quality resonant mode.

to the fact that the capacitor is neutral, on the opposite side we find a charge of the opposite sign (in this example, it is negative). The capacitor is, therefore, charged with an impulsive current so that between the two plates there is a voltage difference equal to $V_0 = -q_0/C$, with C the capacity of this capacitor. The voltage between the two plates produces a wall current I, as shown in the middle part of the figure, which, during its flow, encounters a resistance R due to the finite resistivity of the cavity material. In its turn, this current produces a circular magnetic field and, therefore, a magnetic flux and an inductance L, still between the two plates. The final result is the parallel RLC circuit shown on the right-hand side of the figure.

In this circuit, the voltage across the gap coincides with the voltage between the two parallel plates, that is with the voltage of the capacitor. Due to the parallel RLC circuit, this voltage starts to

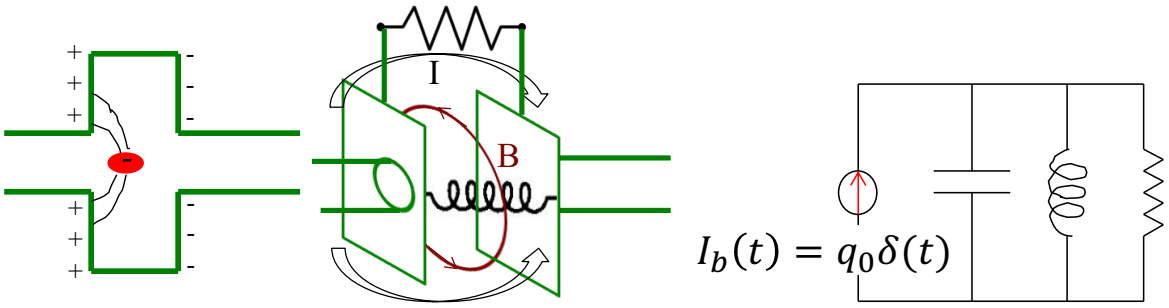

Fig. I.12.25: A pillbox cavity and the equivalent RLC parallel circuit.

oscillate, bouncing the energy between the capacitor and the inductor. Each time, some of this energy is dissipated in the resistance. The time evolution of this voltage can be obtained by solving the following second-order differential equation

$$\ddot{V} + \frac{1}{RC}\dot{V} + \frac{1}{LC}V = 0. \tag{I.12.101}$$

This equation has the form of that of a damped oscillator of the kind

$$\ddot{V} + 2\gamma\dot{V} + \omega_r^2 V = 0 \tag{I.12.102}$$

with

$$\gamma = \frac{1}{2RC} \qquad \omega_r = \frac{1}{\sqrt{LC}}. \tag{I.12.103}$$

At time $t = 0$, the charge q_0 passes through the cavity charging the capacitor with the initial voltage V_0. This voltage, at time $t = 0^+$, produces a current I that initially all flows in the resistance because of the initial infinite opposition of the inductance so that the second starting condition is

$$\dot{V}(t=0^+) = \left.\frac{dV}{dt}\right|_{t=0^+} = \left.\frac{d}{dt}\frac{q}{C}\right|_{t=0^+} = \left.\frac{1}{C}\frac{dq}{dt}\right|_{t=0^+} = -\frac{I(t=0^+)}{C} = -\frac{V_0}{RC}. \tag{I.12.104}$$

With these initial conditions, the solution of the differential equation is

$$V(t) = V_0 e^{-\gamma t}\left[\cos(\omega_n t) - \frac{\gamma}{\omega_n}\sin(\omega_n t)\right] \tag{I.12.105}$$

with

$$\omega_n^2 = \omega_r^2 - \gamma^2. \tag{I.12.106}$$

This voltage can be related to the wakefield. Indeed, if a second (test) charge passes inside the cavity after a time delay $t = -z/c$ (remember that z is negative behind the source charge and a time delay is positive), it changes its energy by the quantity $U(t) = qV(t)$. Since the longitudinal wakefield

is the energy change divided by the two charges, we can write

$$w_{\parallel}(t) = \frac{U(t)}{qq_0} = \frac{V_0}{q_0} e^{-\gamma t} \left[\cos(\omega_n t) - \frac{\gamma}{\omega_n} \sin(\omega_n t) \right]. \tag{I.12.107}$$

Instead of time we use, as the independent variable, z, so that we obtain the wake function of a resonant mode as

$$w_{\parallel}(z) = -\frac{1}{C} e^{\frac{\gamma z}{c}} \left[\cos\left(\omega_n \frac{z}{c}\right) + \frac{\gamma}{\omega_n} \sin\left(\omega_n \frac{z}{c}\right) \right] H(-z). \tag{I.12.108}$$

In writing this last equation, we have considered the causality principle so that this wake is different from zero only behind the source charge $z \leq 0$. This condition is given by the Heaviside step function $H(-z)$. This wake is the one represented in Fig. I.12.23. If γ is large, the exponential decay becomes stronger.

The longitudinal coupling impedance of the resonant mode can be obtained with the Fourier transform of the above wake. This is given by

$$Z_{\parallel}(\omega) = \frac{R_s}{1 - iQ\left(\frac{\omega}{\omega_r} - \frac{\omega_r}{\omega}\right)}, \tag{I.12.109}$$

with the shunt resistance equal to the circuit resistance $R_s = R$, and the quality factor given by $Q = \omega_r/(2\gamma)$. This impedance also corresponds to that of the parallel circuit RLC shown on the right-hand side of Fig. I.12.25. In terms of shunt resistance, quality factor and resonant angular frequency, the wake function can also be written as

$$w_{\parallel}(z) = -\frac{R_s \omega_r}{Q} e^{\frac{\omega_r z}{2Qc}} \left[\cos\left(\omega_n \frac{z}{c}\right) + \frac{\omega_r}{2Q\omega_n} \sin\left(\omega_n \frac{z}{c}\right) \right] H(-z). \tag{I.12.110}$$

For the transverse case, it is possible to demonstrate that we have similar equations. In particular, the transverse dipolar wake function of a resonant mode is written as

$$w_{\perp}(z) = \frac{R_{\perp}\omega_r}{Q} e^{\frac{\gamma z}{c}} \sin\left(\omega_n \frac{z}{c}\right) H(-z), \tag{I.12.111}$$

and the coupling impedance as

$$Z_{\perp}(\omega) = \frac{\omega_n}{\omega} \frac{R_{\perp}}{1 - iQ\left(\frac{\omega}{\omega_r} - \frac{\omega_r}{\omega}\right)}. \tag{I.12.112}$$

I.12.2.10 Broadband impedance models

An important feature of the longitudinal coupling impedance given by Eq. (I.12.109) is that it can also be used as a simplified impedance model of a whole machine for short-range wakefields, assuming $Q \simeq 1$. This is called the Broadband Resonator Impedance model. For example, with $Q = 1$ and a proper choice of R_s and ω_r, the absolute value of $|Z_{\parallel}/n|$ as a function of frequency is represented in Fig. I.12.26. This figure is very similar to that shown on the right-hand side of Fig. I.12.21. The advantage of this model is

that only three parameters (or, even better two, if one considers $Q = 1$) are necessary to describe it, and it can be used to study the collective effects in the longitudinal plane analytically, of course with some approximations.

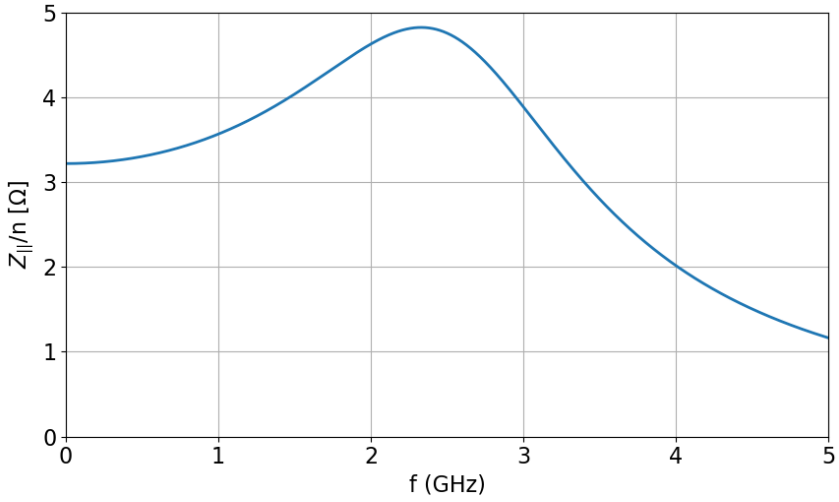

Fig. I.12.26: Absolute value of the broadband resonator impedance as a function of frequency.

An improved version of this model uses two broadband resonators with different shunt impedances and resonant frequencies. Additionally, the quality factor values can be varied.

This is not the only broadband impedance model that has been proposed for the analytical study of collective effects in the longitudinal plane.

Another simplified broadband impedance model is obtained by a phenomenological expansion over $\sqrt{\omega}$ of the different contributions to a machine impedance. By considering only the first two terms of the expansion, we have the so-called RL impedance model, which is

$$Z_{\parallel}(\omega) = R - i\omega L \tag{I.12.113}$$

The resistive term R takes into account the losses of the beam, while the second term, which represents an inductive impedance, gives the low-frequency behaviour typical of tapers, shielded bellows and vacuum ports, small discontinuities as slots, shallow cavities in flanges, and so on. The corresponding wake function is the sum of two terms: the one corresponding to the inverse Fourier transform of the resistive part of the impedance, which is proportional to the Dirac delta function $w_{\parallel}(z) = cR\delta(z)$, while that of the imaginary part (the inductance), which is similar to what we have obtained for the space charge, in particular, it is proportional to the derivative of the Dirac delta function.

I.12.3 Impedance-induced effects

The wake functions and the corresponding coupling impedances are used in beam dynamics studies to determine the so-called impedance-induced effects. This can be carried out with analytical approaches using simplified models, or, in a more rigorous and realistic way, through simulation codes.

In this Section, we will discuss some important effects produced by wakefields that can be ex-

plained with simple analytical models.

I.12.3.1 Energy loss and energy spread

In Section I.12.2.3, with Eq. (I.12.81), we have obtained the energy loss of the whole bunch due to the wakefields. This is one effect of the longitudinal wake that, under some conditions, has to be taken into account because the lost energy must be compensated for by the RF system. For example, in a Linac, the wakefield produced by the interaction of the beam with the fundamental accelerating mode also called the beam loading effect, can limit the maximum energy of the Linac or its maximum current.

Additionally, with Eq. (I.12.78), we have also obtained the energy variation of a charge inside a bunch due to the longitudinal wakefields. This energy variation depends on the position of the charge inside the distribution. As a consequence, this effect generates an energy spread inside the bunch distribution that could reduce the accelerator performance.

As an example of the application of these concepts, let us first evaluate the energy spread and loss of a Gaussian longitudinal distribution of the kind

$$\lambda(s) = \frac{q_{\text{tot}}}{\sqrt{2\pi}\sigma_z} e^{-\frac{s^2}{2\sigma_s^2}}, \tag{I.12.114}$$

with σ_s the rms bunch length, due to the longitudinal space charge wake function of Eq. (I.12.99). We first evaluate the energy lost by a charge inside the distribution. According to Eq. (I.12.78), this is equal to

$$\begin{aligned} U(s) &= -\frac{\ell q q_{\text{tot}}}{4\pi\varepsilon_0\gamma^2\sqrt{2\pi}\sigma_z}\left(1+2\ln\frac{b}{a}\right)\int_{-\infty}^{\infty}\delta'(s-s')e^{-\frac{s'^2}{2\sigma_s^2}}ds' = \\ &= -\frac{\ell q q_{\text{tot}}}{4\pi\varepsilon_0\gamma^2\sqrt{2\pi}\sigma_s}\left(1+2\ln\frac{b}{a}\right)\frac{d}{ds}\left(e^{-\frac{s^2}{2\sigma_s^2}}\right) = \frac{\ell q q_{\text{tot}}}{4\pi\varepsilon_0\gamma^2\sqrt{2\pi}\sigma_s^3}\left(1+2\ln\frac{b}{a}\right)ze^{-\frac{s^2}{2\sigma_s^2}}. \end{aligned} \tag{I.12.115}$$

Observe that the particles in the head of the bunch gain energy ($s > 0$), while those in the tail lose energy. Energy spread can be evaluated, for example, by the difference between the maximum value of $U(s)$ and the minimum value.

From this equation, together with Eq. (I.12.81), we can also obtain the energy lost by the whole bunch due to the space charge. With symmetry considerations, it is possible to show that in this case this energy is zero: the longitudinal space charge produces only an energy spread inside the bunch.

Another example that can be easily evaluated analytically is that of the interaction of a uniform bunch distribution of length ℓ_0, of the kind

$$\lambda(s) = \begin{cases} \dfrac{q}{\ell_0} & -\dfrac{\ell_0}{2} \le s \le \dfrac{\ell_0}{2} \\ 0 & \text{otherwise} \end{cases}, \tag{I.12.116}$$

with the wake function of a resonant HOM that, for simplifying the calculations, we approximate here as

$$w_{\parallel}(z) = -w_0 \cos\left(\omega_r \frac{z}{c}\right) H(-z). \tag{I.12.117}$$

The energy lost by a charge inside a distribution is then

$$U(s) = -\frac{qq_{\text{tot}}w_0}{\ell_0}\int_z^{\ell_0/2}\cos\left[\omega_r\frac{(s-s')}{c}\right]ds' = \frac{qq_{\text{tot}}w_0}{\ell_0}\left.\frac{\sin\left(\omega_r\frac{x}{c}\right)}{\frac{\omega_r}{c}}\right|_0^{s-\ell_0/2} = \\ = -\frac{qq_{\text{tot}}w_0}{2}\left\{\frac{\sin\left[\frac{\omega_r}{c}\left(\frac{\ell_0}{2}-s\right)\right]}{\frac{\omega_r}{c}\frac{\ell_0}{2}}\right\}. \quad \text{(I.12.118)}$$

Exercise 18

Evaluate the energy lost by a charge inside a uniform longitudinal distribution of length ℓ_0 due to a HOM using the exact wake given by Eq. (I.12.108).

As for the space charge case, the energy change due to the interaction of the bunch with a HOM depends on the position of the charge inside the distribution. We can also say that there is an energy spread correlated with the longitudinal position. The maximum energy spread can be evaluated as $U_{\text{max}} - U_{\text{min}}$. Observe that, as expected, if $s = \ell_0/2$, that is, at the head of the bunch, the energy lost is zero due to the causality principle, since a particle in $s = \ell_0/2$ does not see the wake of all particles behind it.

Starting from the above expression we can also evaluate the energy loss due to the whole bunch. According to Eq. (I.12.81) we have

$$U_{\text{bunch}} = -\frac{q_{\text{tot}}^2 w_0}{2\ell_0\left(\frac{\omega_r}{c}\frac{\ell_0}{2}\right)}\int_{-\ell_0/2}^{\ell_0/2}\sin\left[\frac{\omega_r}{c}\left(\frac{\ell_0}{2}-s\right)\right]ds = -\frac{q_{\text{tot}}^2 w_0 c^2}{\omega_r^2\ell_0^2}\left[1-\cos\left(\frac{\omega_r\ell_0}{c}\right)\right]. \quad \text{(I.12.119)}$$

This equation can also be written as

$$U_{\text{bunch}} == -\frac{2q_{\text{tot}}^2 w_0 c^2}{\omega_r^2\ell_0^2}\sin^2\left(\frac{\omega_r\ell_0}{2c}\right) = -\frac{q_{\text{tot}}^2 w_0}{2}\frac{\sin^2\left(\frac{\omega_r\ell_0}{2c}\right)}{\left(\frac{\omega_r\ell_0}{2c}\right)^2}. \quad \text{(I.12.120)}$$

This expression allows us to easily evaluate the limit when $\ell_0 \to 0$. Indeed, since

$$\lim_{x\to 0}\frac{\sin^2(x)}{x^2} = 1, \quad \text{(I.12.121)}$$

we have therefore that

$$\lim_{\ell_0\to 0} U_{\text{bunch}} = -\frac{q_{\text{tot}}^2 w_0}{2}. \quad \text{(I.12.122)}$$

On the other hand, when the bunch length ℓ_0 tends to zero, our bunch distribution becomes a point charge. From the definition of loss factor given by Eq. (I.12.71), we also know that $U(z=0) = -q^2 k_{\parallel}$. We can therefore conclude that

$$k_{\parallel} = \frac{w_0}{2} \quad \text{(I.12.123)}$$

in which we recognize the beam-loading theorem.

I.12.3.2 Single bunch beam break-up in Linacs

I.12.3.2.1 Preliminary considerations: driven oscillator

Before dealing with the beam break-up instability produced by the transverse wakefield, let us first make some preliminary remarks on the motion of a harmonic oscillator driven by an external periodic force. Let us indicate with ω the angular frequency of the harmonic oscillator and with Ω that of the external driving force.

Instead of using time as an independent variable, let us use the position $s = vt$, with v the oscillator velocity (which we consider here equal to the speed of light $v = c$). The equation of motion of the harmonic oscillator can be written as

$$x'' + \frac{\omega^2}{c^2} x = A \cos\left(\frac{\Omega s}{c}\right), \tag{I.12.124}$$

where x'' is the second derivative of the position with respect to s, and A is a constant proportional to the amplitude of the external force. We want to solve this differential equation by considering some given starting conditions. It is convenient to use the complex notation with the condition to retain only the real part of the final solution.

The above equation is a second-order non-homogeneous differential equation with a solution equal to the sum of the complementary solution and a particular one

$$x(s) = x^f(s) + x^d(s) \tag{I.12.125}$$

with f the solution of the 'free' oscillations, and d the 'driven' one. In complex notation we have

$$x^f(s) = \tilde{x}^f_m e^{i\frac{\omega s}{c}} \qquad x^d(s) = \tilde{x}^d_m e^{i\frac{\Omega s}{c}}, \tag{I.12.126}$$

which, substituted in the differential equation, yields

$$\left(\omega^2 - \Omega^2\right) \tilde{x}^d_m e^{i\frac{\Omega s}{c}} = c^2 A e^{i\frac{\Omega s}{c}}, \tag{I.12.127}$$

that gives

$$x^d(s) = \frac{c^2 A}{\omega^2 - \Omega^2} e^{i\frac{\Omega s}{c}}. \tag{I.12.128}$$

In order to also find the amplitude $\tilde{x}^f_m$ we need to specify the initial conditions. For simplicity let us assume that the harmonic oscillator is at rest at $s = 0$. This means that

$$x^f(s = 0) = -x^d(s = 0), \tag{I.12.129}$$

that is

$$\tilde{x}^f_m = -\frac{c^2 A}{\omega^2 - \Omega^2}, \tag{I.12.130}$$

so that

$$x(s) = \frac{c^2 A}{\omega^2 - \Omega^2} \left(e^{i\frac{\Omega s}{c}} - e^{i\frac{\omega s}{c}} \right). \tag{I.12.131}$$

The real part of this expression is then

$$x(s) = \frac{c^2 A}{\omega^2 - \Omega^2} \left[\cos\left(\frac{\Omega s}{c}\right) - \cos\left(\frac{\omega s}{c}\right) \right]. \tag{I.12.132}$$

In the case of general initial conditions, we can add, to the above equation, a sinusoidal term satisfying them, so that we have

$$x(s) = X_0 \cos\left(\frac{\omega s}{c} + \theta_0\right) + \frac{c^2 A}{\omega^2 - \Omega^2} \left[\cos\left(\frac{\Omega s}{c}\right) - \cos\left(\frac{\omega s}{c}\right) \right], \tag{I.12.133}$$

where X_0 and θ_0 depend on the initial conditions. The above expressions are suitable for deriving the response of the oscillator driven at a frequency close to or equal to the resonant frequency. For this purpose, let us define two frequencies

$$\delta = \omega - \Omega, \qquad \bar{\omega} = \frac{\omega + \Omega}{2}. \tag{I.12.134}$$

From them, we can write

$$\omega = \bar{\omega} + \frac{\delta}{2}, \qquad \Omega = \bar{\omega} - \frac{\delta}{2}, \qquad \omega^2 - \Omega^2 = (\omega + \Omega)(\omega - \Omega) = 2\bar{\omega}\delta. \tag{I.12.135}$$

By using the rules of the cosine and sine of the sum of two angles, the equation of motion of the forced harmonic oscillator (I.12.132) can then be written as

$$\begin{aligned} x(s) = \frac{c^2 A}{2\bar{\omega}\delta} \Bigg[& \cos\left(\frac{\bar{\omega} s}{c}\right) \cos\left(\frac{\delta s}{2c}\right) + \sin\left(\frac{\bar{\omega} s}{c}\right) \sin\left(\frac{\delta s}{2c}\right) \\ & - \cos\left(\frac{\bar{\omega} s}{c}\right) \cos\left(\frac{\delta s}{2c}\right) + \sin\left(\frac{\bar{\omega} s}{c}\right) \sin\left(\frac{\delta s}{2c}\right) \Bigg] = \frac{c^2 A}{\bar{\omega}\delta} \sin\left(\frac{\delta s}{2c}\right) \sin\left(\frac{\bar{\omega} s}{c}\right). \end{aligned} \tag{I.12.136}$$

This expression is interesting when ω and Ω are close to each other, that is when the external driving force frequency is close to the resonant one. In this case, we recognize in the last expression the product of two sinusoids: one oscillating at a low frequency $\delta/2$, and the other one at a higher frequency $\bar{\omega}$ (very close to that of the free harmonic oscillator and to that of the external driving force). The first produces an amplitude modulation of the faster oscillations at the frequency $\bar{\omega}$. The result is a beating between the two frequencies of the harmonic oscillator and of the external driving force, as represented in Fig. I.12.27.

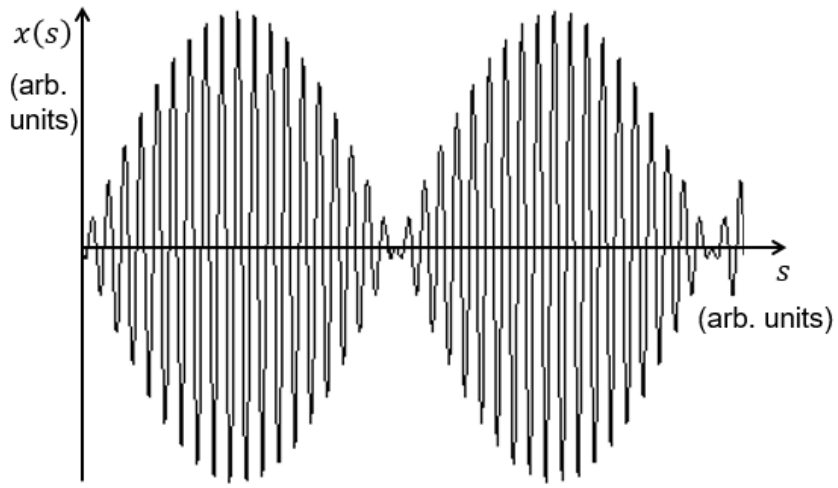

Fig. I.12.27: Amplitude modulated oscillations of a harmonic oscillator with an external driving force having a frequency close to the resonant one.

The same expression can also be written as

$$x(s) = \frac{cAs}{2\bar{\omega}} \sin\left(\frac{\bar{\omega}s}{c}\right) \frac{\sin\left(\frac{\delta s}{2c}\right)}{\frac{\delta s}{2c}}. \tag{I.12.137}$$

In this way, it is easy to evaluate the limit for $\Omega \to \omega$, that is, when the harmonic oscillator is driven in resonance. Indeed, if $\delta \to 0$, the ratio $\sin(\delta)/\delta = 1$ and we remain with

$$\lim_{\delta \to 0} x(s) = \frac{cAs}{2\bar{\omega}} \sin\left(\frac{\bar{\omega}s}{c}\right). \tag{I.12.138}$$

In this condition, the harmonic oscillator increases linearly its amplitude with s as shown in Fig. I.12.28. Of course, in this case, we have used the solution with the initial conditions $x(s=0) = 0$ and $x'(s=0) = 0$. For more general initial conditions, in the above equation, we must add a sinusoidal oscillation as the first term on the right-hand side of Eq. (I.12.133), so that we have

$$x(s) = X_0 \cos\left(\frac{\omega s}{c} + \theta_0\right) + \frac{cAs}{2\bar{\omega}} \sin\left(\frac{\bar{\omega}s}{c}\right). \tag{I.12.139}$$

I.12.3.2.2 Single bunch beam break-up

In this Section, we discuss an instability produced by the transverse wakefields that can be very dangerous for a Linac. The study is carried out considering a single bunch with an injection offset in an accelerating structure of a Linac, for example, due to some misalignments.

As a result of the focusing quadrupoles, the bunch executes betatron oscillations, and, due to the transverse displacement, it excites transverse wakefields. The head of the bunch undergoes unperturbed

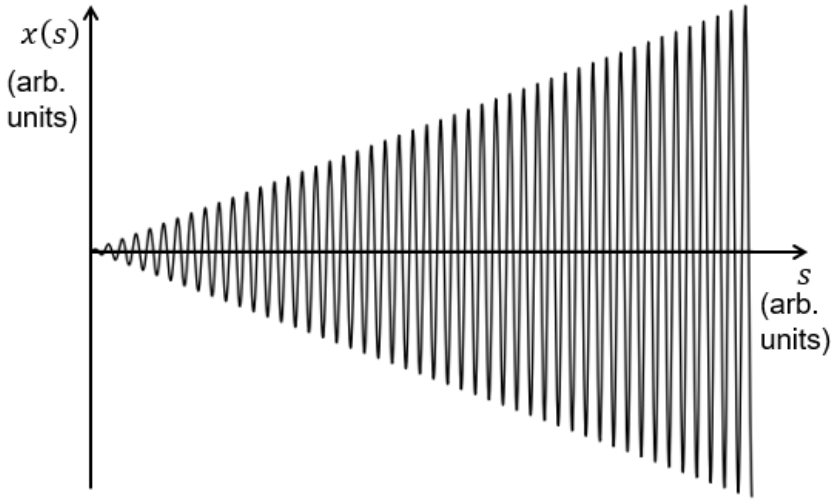

Fig. I.12.28: Amplitude modulated oscillations of a harmonic oscillator with an external driving force on resonance.

oscillations because, according to the causality principle, it is not affected by the transverse wake. However, the trailing charges in the tail can be deflected by the wake of the head.

Since the wakefield force is proportional to the offset of the leading particles, it acts as an external driving force in resonance at the betatron frequency with the tail oscillations. The amplitude of these oscillations will then increase with distance, as we have discussed in the previous Section. The result is that the tail of the bunch distorts, assuming a kind of "banana shape", as represented in Fig. I.12.29. This process is called single-bunch beam break-up [7], and it was first observed at SLAC in 1966 [8].

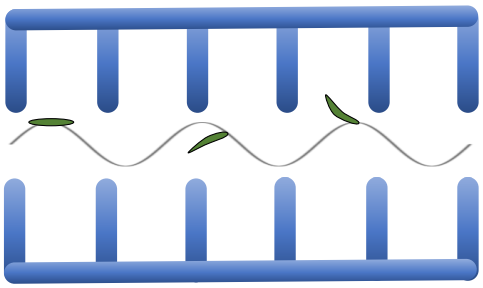

Fig. I.12.29: Single bunch beam break-up.

Similarly, any beam offset or structure misalignment will excite long-range wakefields, which will then cause subsequent bunches to be deflected. There could be then also a coupling in the motion of the different bunches, which are more and more deflected as they proceed along the Linac in a process called multi-bunch or cumulative beam break-up.

Even if the particles are not lost hitting the beam pipe walls, the beam emittance can be greatly increased.

In order to understand and analytically treat the effect, we consider a simple model with only

two charges: $q_1 = Nq/2$ (source charge equal to the half bunch in the head concentrated in a single point), and $q_2 = q$ (test charge corresponding to a single charge in a position in the tail). The model is represented in Fig. I.12.30, and it is called a two-particle model.

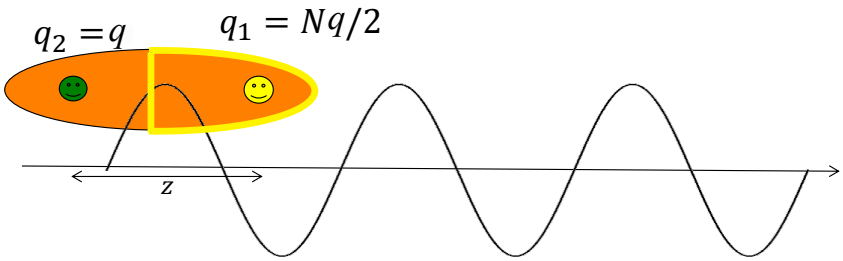

Fig. I.12.30: Two-particle model for beam break-up study.

The source charge, at the head of the bunch, since the transverse wake in $z = 0$ is zero, executes unperturbed free betatron oscillations of the kind

$$y_1(s) = \hat{y}_1 \cos\left(\frac{\omega_y}{c}s\right), \tag{I.12.140}$$

with ω_y the betatron angular frequency. Observe here that, since we are in a Linac, we do not use the term betatron tune.

The test charge, at a distance z from the source, in a structure of length L_w, according to the definition of Eq. (I.12.68), experiences a transverse deflecting kick proportional to the displacement y_1, and dependent on the distance z

$$y_1(s)M_y(z) = \int_0^{L_w} F_y ds =< F_y(y_1, z) > L_w, \tag{I.12.141}$$

where, for the last expression, we have used the definition of the mean value theorem for integrals. We consider the transverse deflecting self-field force $< F_y >$ as the average transverse force in the structure of length L_w. By using the definition of transverse dipolar wakefield given by Eq. (I.12.70), since $q_0 = qN/2$, we can write

$$< F_y(y_1, z) >= \frac{Nq^2}{2L_w} w_y(z) y_1(s). \tag{I.12.142}$$

The transverse equation of motion for the test charge q, affected by the self-field force, is similar to that of Eq. (I.12.47), with K substituted, as for the betatron oscillation of the source, by $(\omega_y/c)^2$, so that

$$y_2''(s) + \left(\frac{\omega_y}{c}\right)^2 y_2(s) = \frac{1}{\beta^2 E_0} < F_y(y_1, z) >= \frac{Nq^2}{2\beta^2 E_0 L_w} w_y(z)\hat{y}_1 \cos\left(\frac{\omega_y}{c}s\right). \tag{I.12.143}$$

This is the typical equation of a harmonic oscillator driven at the resonant frequency as the one discussed in the previous Section I.12.3.2.1. In this case, the external force is due to the transverse wakefield produced by the displacement of the source charge. The solution is given by the superposition

of the "free" oscillations and forced oscillations, which, being driven at the resonant frequency, grow linearly with s according to Eq. (I.12.138). The solution of this differential equation is, therefore, similar to that of Eq. (I.12.139), that is

$$y_2(s) = \hat{y}_1 \cos\left(\frac{\omega_y}{c}s + \theta_0\right) + \frac{cNq^2 s w_y(z)}{4\omega_y \beta^2 E_0 L_w}\hat{y}_1 \sin\left(\frac{\omega_y}{c}s\right), \tag{I.12.144}$$

for which we have supposed that the initial displacement of the bunch tail is the same as that of the bunch head, that is $\hat{y}_2 = \hat{y}_1$.

The second term on the right-hand side of the equation is due to the on-resonance wakefield force. At the beginning of the Linac, for very small values of s, this term is still negligible and we have free oscillations that start slowly to increase as shown in Fig. I.12.31, while, when the driving term dominates, we have oscillations similar to those shown in Fig. I.12.28

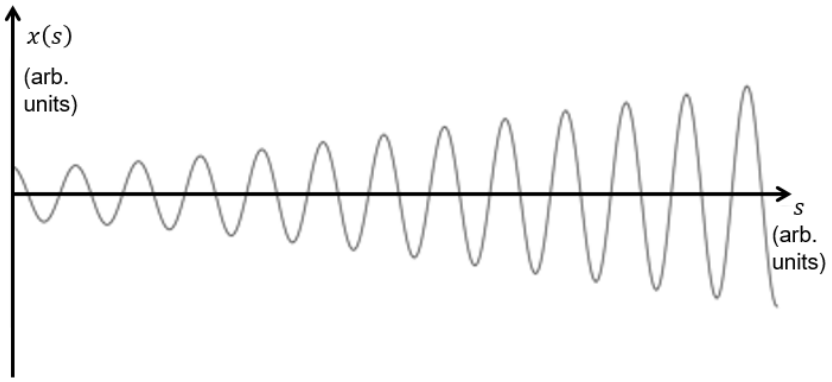

Fig. I.12.31: Betatron oscillations of a charge in a bunch tail excited by the transverse wakefield of the head at the beginning of a Linac.

At the end of a Linac of length L_L, the increase of the amplitude oscillations of the tail with respect to the head of the bunch is

$$\frac{y_2(L_L) - \hat{y}_1}{\hat{y}_1} = \frac{cNqL_L w_y(z)}{4\omega_y \beta^2 (E_0/q) L_w}. \tag{I.12.145}$$

For Linacs with ultra-relativistic electron beams, we can assume $\beta = 1$. If the transverse wake is given per cell, the relative displacement of the tail with respect to the head of the bunch depends on the number of cells. It also depends, of course, on the focusing strength through frequency ω_y.

Of course, if at the end of the Linac, the transverse displacement of the tail is much lower than the bunch dimension, that is $y_2(L_L) \ll \sigma_y$, then, the beam break-up effect can be neglected. This condition occurs when

$$\frac{cNqL_L w_y(z)}{4\omega_y \beta^2 (E_0/q) L_w}\hat{y}_1 \ll \sigma_y. \tag{I.12.146}$$

Observe that we can neglect this instability when the initial transverse displacement of the bunch head $\hat{y}_1$ is very small, when the transverse wake per unit of length $w_y(z)/L_w$ is weak, when the Linac is short, at high energy, or when the focusing effect of the quadrupole (proportional to ω_y) is strong.

Exercise 19

Consider an electron beam in a Linac at 1 GeV without acceleration. Obtain the growth of the oscillation amplitude of the tail with respect to the head after 3 km if: $N = 5 \times 10^{10}$, $w_y(z = -1\text{mm}) = 63$ V/(pC m), $L_w = 3.5$ cm, $k_y = 0.06$ 1/m.

Exercise 20

With constant acceleration in the Linac, if the beam energy can be written as $E_f = E = 0 + gL_L$, with g the acceleration gradient, the growth of the oscillation amplitude of the tail with respect to the head is the same as that of the constant energy case multiplied by a factor equal to

$$F = \frac{E_0}{E_f} \ln \frac{E_f}{E_0}.$$

Evaluate the growth of the oscillations with the same beam of the previous exercise that is now accelerated from an initial energy of 1 GeV with a gradient $g = 16.7$ MeV/m.

I.12.3.2.3 BNS damping

This instability can be quite harmful and hard to take under control even at high energy, with a strong focusing effect, and after a careful injection and steering.

A simple and smart method to cure it has been proposed observing that the large oscillation amplitude of the bunch tail is generated by the resonant driving force of the bunch head.

If the tail and the head of the bunch oscillate with different frequencies, this effect can be significantly mitigated.

Let us assume that the tail oscillates with a frequency $\omega_y + \Delta\omega_y$. Then the equation of motion (I.12.143) becomes:

$$y_2''(s) + \left(\frac{\omega_y + \Delta\omega_y}{c}\right)^2 y_2(s) = \frac{Nq^2}{2\beta^2 E_0 L_w} w_y(z) \hat{y}_1 \cos\left(\frac{\omega_y}{c} s\right). \tag{I.12.147}$$

In this case, we are off-resonance and, according to what we have discussed in the previous Section I.12.3.2.1, we have beats so that, from Eq. (I.12.133), the solution can now be written as

$$y_2(s) = \hat{y}_1 \cos\left(\frac{\omega_y + \Delta\omega_y}{c} s\right) + \frac{c^2 N q^2 w_y(z)}{4\omega_y \Delta\omega_y \beta^2 E_0 L_w} \hat{y}_1 \left[\cos\left(\frac{\omega_y}{c} s\right) - \cos\left(\frac{\omega_y + \Delta\omega_y}{c} s\right)\right]. \tag{I.12.148}$$

In writing this solution, we have supposed that, at injection, the head and tail of the bunch have the same offset, that is, $\hat{y}_2 = \hat{y}_1$, and there is no divergence ($\theta_0 = 0$). The oscillations of the tail are then of the type of those shown in Fig. I.12.32.

If we now choose $\Delta\omega_y$ such that

$$\frac{c^2 N q^2 w_y(z)}{4\omega_y \Delta\omega_y \beta^2 E_0 L_w} = 1, \tag{I.12.149}$$

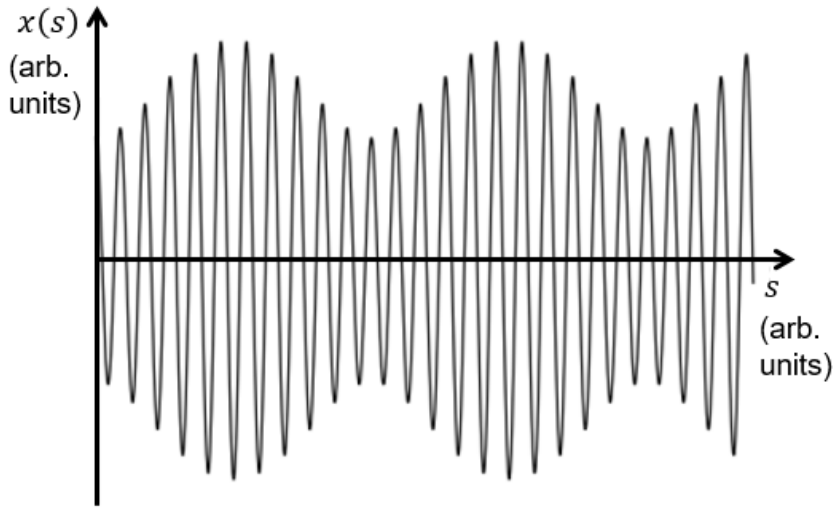

Fig. I.12.32: Betatron oscillations of a charge in a bunch tail excited by the transverse wakefield of the head in case of betatron frequency shift.

that is

$$\Delta\omega_y = \frac{c^2 N q^2 w_y(z)}{4\omega_y \beta^2 E_0 L_w}, \tag{I.12.150}$$

then we remain with

$$y_2(s) = \hat{y}_1 \cos\left(\frac{\omega_y}{c} s\right) = y_1(s), \tag{I.12.151}$$

that is the head and the tail oscillate with the same amplitude and the instability is suppressed.

This method is called BNS damping, from the names of Balakin, Novokhatsky, and Smirnov who first proposed it [9].

The extra focusing acting on the tail of the bunch can be obtained, for example, by using a radio-frequency quadrupole (RFQ), a device in which the head and the tail see a different focusing strength, or by creating a correlated energy distribution along the bunch, which, because of the chromaticity, induces a spread in the betatron frequencies. An energy spread correlated with the longitudinal position is attainable, for example, with the external accelerating voltage or with the longitudinal wakefields.

I.12.3.3 Instabilities in circular accelerators

The study of impedance-induced instabilities in particle accelerators, and in particular for circular machines, started around the mid-end 1960s. The first works on this topic were conducted by V. Vaccaro [10] and A. M. Sessler [11], who described the initial concepts of dispersion relations in the same works where the concept of coupling impedance was introduced. Subsequently, over the course of more than 50 years, a considerable amount of research has been conducted in this field, with numerous papers published on various aspects related to impedance-induced instabilities.

The simplest method that could be followed to study the effects of self-induced electromagnetic fields on beam dynamics is that of introducing the self-induced forces in the motion of a single particle. In practice, this is not possible because a bunch generally contains $10^{10} - 10^{12}$ particles, so the same number

of differential equations (corresponding to Newton's second law) should be solved in a self-consistent way. Consequently, alternative methods must be used to deal with the so-called impedance-induced instabilities.

As a consequence, two approaches are generally followed:

- At one extreme, we can use a continuous distribution function describing the motion of a beam as a superposition of coherent modes of oscillation. This leads to the Vlasov equation [12] (or Fokker Plank [13]) and to the analytical and numerical tools developed to solve it (as the so-called Vlasov solvers [14, 15]). The Vlasov equation is shortly presented in Appendix I.12.D.2;
- On the opposite side, we can simplify the problem and reduce the number of equations by using simulation codes, which track, in the time domain, about $10^6 - 10^7$ macro-particles, taking into account the wake function or the coupling impedance, examples can be found in Ref. [16].

We have seen that the wakefields, defined by Eqs. (I.12.69) and (I.12.70), produce an energy change in the longitudinal direction, while they give a deflection kick in the transverse plane. Therefore, it is convenient to separate the study of beam dynamics and collective effects in the longitudinal and transverse planes.

Additionally, we have also discussed short-range and long-range wakefields. Classically, the study of beam dynamics with collective effects is split into longitudinal, transverse, single, and multi-bunch.

For example, the main longitudinal effects of short-range wakefields are:

- Potential well distortion and deformation of the longitudinal distribution;
- Longitudinal emittance growth, microwave instability;

while the long-range wakefields give

- Robinson instability due to the RF fundamental mode;
- Coupled bunch instability due to HOMs.

The analytical study of these effects with the Vlasov equation is beyond the scope of this lecture. However, in order to give an idea of the kind of instabilities that may occur in a circular accelerator, we describe, in the next session, the Robinson instability.

I.12.3.3.1 Robinson instability due to the RF fundamental mode

Let us consider the real part of the RF fundamental mode impedance and a bunch with nominal revolution period T_0. The bunch spectrum has lines every ω_0 (for simplicity, we suppose that the bunch is a point charge), and its lost energy due to the interaction with the mode is proportional to the real part of the impedance evaluated at the angular frequency $\omega_{\mathrm{RF}} = h\omega_0$, where h, already introduced in Eq. (I.12.63), is the harmonic number. The other frequencies, at distances multiples of ω_0 from ω_{RF}, find a value of the mode impedance so small that it can be neglected. It is important to note that the cavity resonant frequency ω_r can be slightly detuned with respect to the RF frequency ω_{RF} so that they do not necessarily coincide. Actually, this is realized on purpose for damping the Robinson instability as we will see.

The phenomenological description of the instability (or stability) is the following. First, suppose that we have a synchronous beam. In Fig. I.12.33 we have represented the real part of the fundamental mode impedance with its resonant frequency ω_r slightly below the frequency $h\omega_0$. The bunch energy loss due to the mode, together with other possible losses (for example those due to the synchrotron radiation), is compensated in the cavity by the external RF voltage. The synchronous bunch is at equilibrium at each turn.

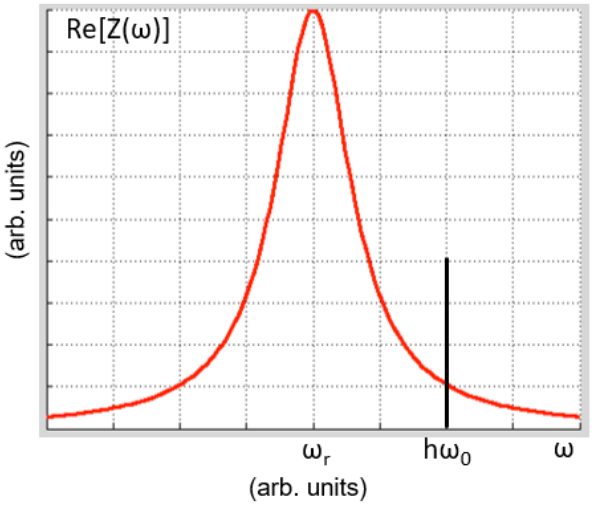

Fig. I.12.33: Real part of the frequency of the fundamental mode and bunch spectrum line of the synchronous particle.

Let us suppose now that, for example, the bunch is not at equilibrium, but it is performing synchrotron oscillations, and the machine operates below transition energy. During a part of these oscillations, the bunch has an energy larger than that of the synchronous particle. Its revolution period is then lower than T_0 and the frequency larger than ω_0.

Therefore, the spectrum line is now at a value greater than $h\omega_0$. From the figure, we see that the resistance found by this bunch is smaller than that at $h\omega_0$, and this produces an energy loss lower than that of the synchronous particle (we have a vertical line of the bunch spectrum shifted a bit on the right side with respect to the black line of the figure). If the bunch gains in the cavity the same energy as that of the synchronous particle, this would lead to extra energy of the bunch that is not compensated by the corresponding loss.

This means that the bunch will have even higher energy with respect to the synchronous particle, thus increasing its oscillation amplitude with the result of an unstable bunch. On the other hand, above transition energy, the opposite situation occurs and the mode impedance has a stabilizing effect. If $h\omega_0 < \omega_r$ we have stability below the transition energy and instability above it. This is called Robinson instability: for example, above transition, detuning the resonant frequency of the mode slightly below $h\omega_0$ gives a stabilizing effect.

This qualitative behaviour can be described analytically. Let us recover the longitudinal equations of motion. Let us suppose that we have a bunch that we consider as a point charge, coinciding with its

centre of mass. Let us also suppose to have a constant energy circular machine (storage ring), and let us ignore radiation damping.

The differential equations of motion in the longitudinal plane can then be written as

$$\frac{d\phi}{dt} = -\frac{h\eta}{R_0 p_0}\Delta E \tag{I.12.152}$$

and

$$\frac{d\Delta E}{dt} = \frac{qV_{\mathrm{RF}}}{T_0}\left(\sin\phi - \sin\phi_s\right), \tag{I.12.153}$$

with ΔE the energy variation with respect to the synchronous particle.

Combining these two equations, for small amplitude oscillations, we obtain a second-order differential equation similar to that of Eq. (I.12.63) but, in this case, we write it in the time domain as

$$\frac{d^2\Delta\phi}{dt^2} + \omega_s^2\Delta\phi = 0, \tag{I.12.154}$$

with ω_s given by Eq. (I.12.64). For stability reasons, we must satisfy the condition $\eta\cos\phi_s > 0$. This is the equation that describes the synchrotron oscillations.

The solution of this harmonic oscillator equation can be written as

$$\Delta\phi = \Delta\phi_{\mathrm{max}}\cos\left(\omega_s t + \theta_0\right). \tag{I.12.155}$$

In this simple equation, it is possible to additionally include the effect of the wakefield produced by the RF fundamental mode. Indeed this can be represented through the loss factor and can be written as an additional term on the right-hand side of Eq. (I.12.153) describing the energy variation with time. Without going into the details of the calculations, we give here only the result. By considering small oscillations, the differential equation of motion becomes now

$$\frac{d^2\Delta\phi}{dt^2} + 2\alpha_r\frac{d\Delta\phi}{dt} + \omega_s^2\Delta\phi = 0. \tag{I.12.156}$$

We have here an additional term proportional to α_r and to the first time derivative of $\Delta\phi$ having a form similar to that of Eq. (I.12.102), which gives an amplitude of the oscillations depending exponentially with time. Indeed, if $\alpha_r < \omega_s$, by writing $\omega_n = \sqrt{\omega_s^2 - \alpha_r^2}$, the solution is

$$\Delta\phi = \Delta\phi_{\mathrm{max}}e^{-\alpha_r t}\cos\left(\omega_s t + \theta_0\right). \tag{I.12.157}$$

The value of α_r is given by

$$\alpha_r = \frac{q_{\mathrm{tot}}\eta h\omega_0}{2\omega_s(E_0/q)T_0^2}Re[\Delta Z], \tag{I.12.158}$$

where $Re[\Delta Z]$ is the difference between the real part of the impedance of the fundamental mode evalu-

ated at $h\omega_0 \pm \omega_s$, that is

$$Re[\Delta Z] = Re\left[Z(h\omega_0 + \omega_s)\right] - Re\left[Z(h\omega_0 - \omega_s)\right]. \tag{I.12.159}$$

From the above equations, we can see that the sign of α_r depends on both η and $Re[\Delta Z]$. If this is positive, according to Eq. (I.12.157), we have exponentially damped oscillations; otherwise we have instability.

For example, if we are above transition energy, $\eta < 0$, so that, in order to have stability, we must have that $[Z(h\omega_0 + \omega_s)] < Re\left[Z(h\omega_0 - \omega_s)\right]$. This situation occurs when the RF frequency $\omega_{\mathrm{RF}} = h\omega_0$ is larger than the mode resonant frequency, as shown in Fig.I.12.34. Of course, we can have different combinations of η and $Re[\Delta Z]$. These conclusions are the same as those we have discussed in the phenomenological description.

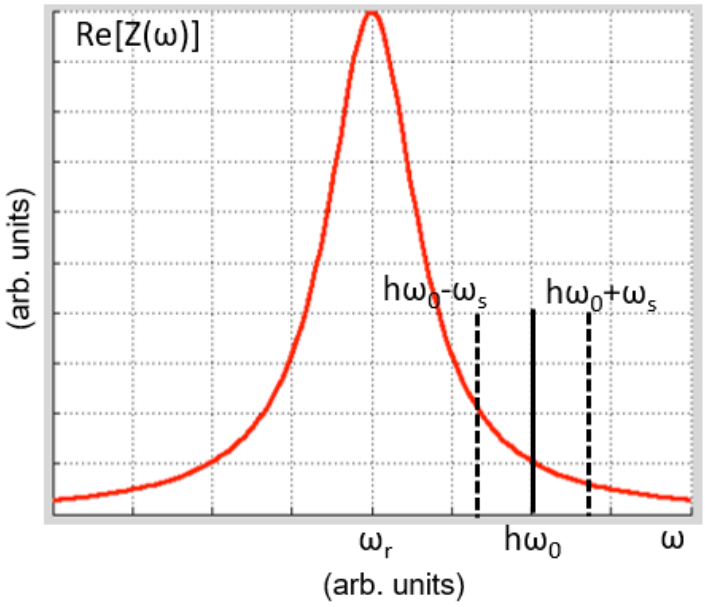

Fig. I.12.34: Real part of the frequency of the fundamental mode and bunch spectrum line of the synchronous particle.

I.12.4 Solutions to the exercises

Exercise 1

By considering a cylinder of radius $r > a$, according to the Gauss theorem, we have

$$2\pi r E_r \ell = \frac{\rho \pi a^2 \ell}{\varepsilon_0} = \frac{\lambda \ell}{\varepsilon_0} \quad \rightarrow \quad E_r = \frac{\lambda}{2\pi\varepsilon_0 r}.$$

Analogously, from the Ampere law, we can write

$$2\pi r B_\theta = \mu_0 J \pi a^2 = \mu_0 v \lambda \quad \rightarrow \quad B_\theta = \frac{\beta}{c}\frac{\lambda}{2\pi\varepsilon_0 r},$$

from which

$$F_r = q\left(E_r - vB_\theta\right) = \frac{qE_r}{\gamma^2} = \frac{q\lambda}{2\pi\varepsilon_0\gamma^2 r}.$$

Exercise 2

$$2\pi r E_r \ell = \frac{\lambda_0}{2\pi\varepsilon_0\sigma_r^2}\ell\int_0^r e^{-\frac{r'^2}{2\sigma_r^2}}2\pi r' dr' = \frac{\lambda_0\ell}{\varepsilon_0}\left(1 - e^{-\frac{r^2}{2\sigma_r^2}}\right),$$

from which

$$E_r = \frac{\lambda_0}{2\pi\varepsilon_0}\frac{1 - e^{-\frac{r^2}{2\sigma_r^2}}}{r}.$$

Exercise 3

Consider a reference system moving with the same speed as the charge. In this reference system, the charge is at rest close to a conducting plane. This is equivalent as having an image charge of opposite sign at distance $2d$ producing, on the charge, an attractive force equal to

$$F_0 = \frac{q^2}{4\pi\varepsilon_0(2d)^2}.$$

If we transform the transverse force in the laboratory system, according to the transformation of the forces, we have

$$F = \frac{F_0}{\gamma} = \frac{q^2}{4\pi\varepsilon_0\gamma(2d)^2}.$$

Exercise 4

Similarly to Eq. (I.12.10), we have

$$E_r(r,s) = \frac{\lambda(s)}{2\pi\varepsilon_0 a^2}r \qquad B_\theta(r,s) = \frac{\beta}{c}\frac{\lambda(s)}{2\pi\varepsilon_0 a^2}r,$$

so that

$$F_r(r,s) = q(E_r - vB_\theta) = q\frac{\lambda(s)}{2\pi\varepsilon_0\gamma^2 a^2}r.$$

Exercise 5

Since the circular vacuum chamber does not modify the electric and magnetic field lines for an ultra-relativistic beam with a non-uniform longitudinal distribution, the force is simply given by Eq. (I.12.25) with $\lambda(s)$ substituted by the three longitudinal distributions, which are generally used for the study of

- Electron bunch instabilities in the case of Gaussian distribution,
- Proton bunch instabilities in the case of parabolic distribution,
- Coasting beam instabilities in the case of sinusoidal modulations.

Exercise 6

The magnetic field lines must be orthogonal to the plates' surface. The image magnetic field can be obtained by considering image currents with the same sign as shown in Fig. I.12.35.

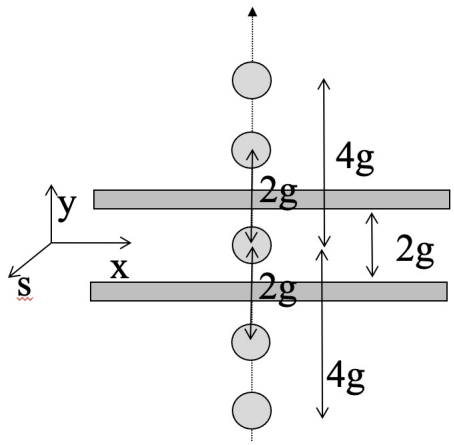

Fig. I.12.35: Image currents related to Exercise 6.

Suppose that a charge inside the beam is in a generic vertical position y with $x = 0$. If all the currents exit out of the figure, then the magnetic field due to the image currents can be written as

$$B_x^{\text{im}} = \frac{\mu_0 \beta c \lambda(s)}{2\pi} \sum_{n=1}^{\infty} \left(\frac{1}{2ng - y} - \frac{1}{2ng + y} \right) = \frac{\mu_0 \beta c \lambda(s)}{2\pi} \sum_{n=1}^{\infty} \frac{2y}{(2ng)^2 - y^2}$$
$$\simeq \frac{\mu_0 \beta c \lambda(s)}{4\pi g^2} y \sum_{n=1}^{\infty} \frac{1}{n^2} = \frac{\mu_0 \beta c \lambda(s)}{4\pi g^2} \frac{\pi^2}{6} y.$$

For the vertical magnetic field, we can use the component of the curl equation along z

$$\left(\nabla \times \mathbf{B}^{\text{im}}\right)_z = 0 \quad \rightarrow \quad \frac{\partial B_x^{\text{im}}}{\partial y} = \frac{\partial B_y^{\text{im}}}{\partial x} \quad \rightarrow \quad B_y^{\text{im}} = \frac{\mu_0 \beta c \lambda(s)}{4\pi g^2} \frac{\pi^2}{6} x.$$

Exercise 7

With the condition that the magnetic field lines must be tangent to the parallel plates, as shown in Fig. I.12.6, we obtain an infinite series of alternating currents. Following the same method that we have used for the electric field in the DC case, we have now

$$\tilde{B}_x^{\text{im}} = \frac{\mu_0 \tilde{I}}{2\pi} \sum_{n=1}^{\infty} (-1)^n \left(\frac{1}{2nh - y} - \frac{1}{2nh + y} \right) = \frac{\mu_0 \beta c \tilde{\lambda}(s)}{2\pi} \sum_{n=1}^{\infty} (-1)^n \frac{2y}{4h^2 n^2 - y^2}$$
$$\simeq \frac{\beta}{c} \frac{\tilde{\lambda}(s)}{4\pi\varepsilon_0 h^2} y \sum_{n=1}^{\infty} (-1)^n \frac{1}{n^2} = \frac{\beta}{c} \frac{\tilde{\lambda}(s)}{4\pi\varepsilon_0 h^2} y \left(-\frac{\pi^2}{12} \right) = -\frac{\beta}{c} \tilde{E}_y^{\text{im}},$$

and

$$\left(\nabla \times \tilde{\mathbf{B}}^{\text{im}} \right)_z = 0 \quad \rightarrow \quad \frac{\partial \tilde{B}_x^{\text{im}}}{\partial y} = \frac{\partial \tilde{B}_y^{\text{im}}}{\partial x} \quad \rightarrow \quad \tilde{B}_y^{\text{im}} = \frac{\beta}{c} \tilde{E}_x^{\text{im}}.$$

Exercise 8

$f_0 = 1/2$, $f_1 = \pi^2/48$, $f_2 = \pi^2/24$.

Exercise 9

The electric field inside a uniform cylindrical beam of radius a is given by Eq. (I.12.8), while, outside the distribution, it is given by the solution of Exercise 1. As a consequence, Eq. (I.12.41) becomes

$$E_s(r, s) = -\frac{1}{2\pi\varepsilon_0} \frac{\partial \lambda(s)}{\partial s} \left[\int_r^a \frac{r'}{a^2} dr' + \int_a^b \frac{1}{r'} dr' \right] = -\frac{q}{4\pi\varepsilon_0} \frac{\partial \lambda(s)}{\partial s} \left(1 - \frac{r^2}{a^2} + 2 \ln \frac{b}{a} \right).$$

Exercise 10

Gaussian distribution:

$$\frac{d\lambda}{ds} = -\frac{Nq}{\sqrt{2\pi}\sigma_s^3} z e^{-\frac{s^2}{2\sigma_s^2}},$$

$$F_s(r, s) = qE_s(r, s) = \frac{Nq^2}{4\pi\sqrt{2\pi}\varepsilon_0 \gamma^2 \sigma_s^3} \left(1 - \frac{r^2}{a^2} + 2 \ln \frac{b}{a} \right) s e^{-\frac{s^2}{2\sigma_s^2}}.$$

Observe that this force is positive on the head of the bunch ($s > 0$) and negative on the tail.

Parabolic distribution:

$$\frac{d\lambda}{ds} = -\frac{12Nq}{l_0^3} s,$$

$$F_s(r, s) = qE_s(r, s) = \frac{12Nq^2}{4\pi\varepsilon_0 \gamma^2 l_0^3} \left(1 - \frac{r^2}{a^2} + 2 \ln \frac{b}{a} \right) s.$$

Observe that this force is positive on the head of the bunch ($s > 0$) and negative on the tail.

Sinusoidal modulation of a coasting beam:

$$\frac{d\lambda}{ds} = -\Delta\lambda k_s \sin(k_s s),$$

$$F_s(r,s) = qE_s(r,s) = \frac{\Delta\lambda k_s q}{4\pi\varepsilon_0\gamma^2}\left(1 - \frac{r^2}{a^2} + 2\ln\frac{b}{a}\right)\sin(k_s s).$$

Some observations on this force are given in the comments on Exercise 10.

Exercise 11

According to Eq. (I.12.56), we have:

– Gaussian distribution: the maximum tune shift is for $z = 0$ and it is equal to

$$\Delta Q_{\max} = -\frac{r_{e,p}\rho^2}{\gamma^3\beta^2 a^2 Q_{x0}}\frac{N}{\sqrt{2\pi}\sigma_s}.$$

The minimum tune shift is zero when $s \to \infty$. Therefore,

$$\Delta Q_{spread} = \Delta Q_{\max} - \Delta Q_{\min} = \Delta Q_{\max}.$$

– Parabolic distribution: the maximum tune shift is for $s = 0$ and it is equal to

$$\Delta Q_{\max} = -\frac{r_{e,p}\rho^2}{\gamma^3\beta^2 a^2 Q_{x0}}\frac{3N}{2l_0}.$$

The minimum tune shift is zero when $s = \pm L_0/2$. Therefore,

$$\Delta Q_{spread} = \Delta Q_{\max} - \Delta Q_{\min} = \Delta Q_{\max}.$$

– Sinusoidal modulation: the maximum tune shift is for $k_s s = 2\pi n$ and it is equal to

$$\Delta Q_{\max} = -\frac{r_{e,p}\rho^2}{q\gamma^3\beta^2 a^2 Q_{x0}}(\lambda_0 + \Delta\lambda).$$

The minimum tune shift is for $k_s s = (2n+1)\pi$ and it is equal to

$$\Delta Q_{\min} = -\frac{r_{e,p}\rho^2}{q\gamma^3\beta^2 a^2 Q_{x0}}(\lambda_0 - \Delta\lambda).$$

Therefore

$$\Delta Q_{spread} = \Delta Q_{\max} - \Delta Q_{\min} = -\frac{2r_{e,p}\rho^2\Delta\lambda}{q\gamma^3\beta^2 a^2 Q_{x0}}.$$

Exercise 12

The emittance is related to the transverse dimension through the relation $a^2 = \varepsilon_x \beta_x$. Moreover,

$$\beta_x = \frac{\lambda_\beta}{2\pi} = \frac{1}{\sqrt{K_x}} = \frac{\rho}{Q_{x0}}.$$

Therefore, for the tune shift, we have

$$\Delta Q_x = -\frac{r_{e,p}\rho}{q\gamma^3\beta^2\varepsilon_x}\lambda(s). \tag{I.12.160}$$

Exercise 13

$$\Delta Q_x = -\frac{1}{4\pi\beta^2 E_0 \varepsilon_x}\oint a^2 \left(\frac{\partial F_x^{\text{self}}(s)}{\partial x}\right)_0 ds.$$

Exercise 14

$$\gamma_i = \frac{1.4 + 0.938}{0.938} = 2.49, \qquad \gamma_f = \frac{2 + 0.938}{0.938} = 3.13,$$

$$\left(\frac{3.13}{2.49}\right)^3 = 1.98.$$

Exercise 15

From Eq. (I.12.99) we have

$$\frac{w_\parallel(z)}{\ell} = -\frac{1}{4\pi\varepsilon_0\gamma^2}\left(1 + 2\ln\frac{b}{a}\right)\frac{d\delta(z)}{dz}.$$

By using Eq. (I.12.79), we have then

$$\frac{U(s)}{\ell} = -q\int_{-\infty}^{\infty}\frac{w_\parallel(s-s')}{\ell}\lambda(s')ds' = -\frac{q}{4\pi\varepsilon_0\gamma^2}\left(1 + 2\ln\frac{b}{a}\right)\int_{-\infty}^{\infty}\frac{d\delta(s-s')}{ds'}\lambda(s')ds' = \\ = -\frac{q}{4\pi\varepsilon_0\gamma^2}\left(1 + 2\ln\frac{b}{a}\right)\frac{d\lambda(s)}{ds},$$

which coincide with Eq. (I.12.43) when $r = 0$. They are the same because, by considering a constant longitudinal force, the product $F_z\ell$ coincides with the energy lost by the charge $U(z)$.

Exercise 16

By using Eq. (I.12.81) with $U(s)$ of the previous result, we have

$$\frac{U_{\text{bunch}}}{\ell} = -\frac{1}{4\pi\varepsilon_0\gamma^2}\left(1+2\ln\frac{b}{a}\right)\int_{-\infty}^{\infty}\frac{d\lambda(s)}{ds}\lambda(s)ds = \frac{1}{4\pi\varepsilon_0\gamma^2}\left(1+2\ln\frac{b}{a}\right)\left[\frac{\lambda(s)^2}{2}\right]_{-\infty}^{\infty} = 0,$$

since the longitudinal distribution is zero at $\pm\infty$. On the other hand, the space charge impedance is purely imaginary, while it is possible to demonstrate that it is the real part of the coupling impedance which is related to the bunch energy losses.

Exercise 17

From Exercise 15, by evaluating the derivative of the Gaussian distribution, we have

$$U(s) = \frac{q\ell}{4\pi\varepsilon_0\gamma^2}\left(1+2\ln\frac{b}{a}\right)\frac{s}{\sqrt{2\pi}\sigma_s^3}e^{-\frac{s^2}{2\sigma_s^2}}.$$

As already discussed in the Section dedicated to the longitudinal space charge, this energy is positive ahead of the bunch and it is negative on the tail. The maximum and minimum energy variation can be found when the derivative of this energy is zero, that is

$$\frac{dU(s)}{ds} = 0 \qquad \rightarrow \qquad s = \pm\sigma_s.$$

We have, therefore,

$$U_{\text{max}} - U_{\text{min}} = 2U_{\text{max}} = \frac{2q\ell}{4\pi\varepsilon_0\gamma^2}\left(1+2\ln\frac{b}{a}\right)\frac{1}{\sqrt{2\pi}\sigma_s^2}e^{-\frac{1}{2}}.$$

Exercise 18

$$U(s) = -\frac{qq_{\text{tot}}w_0}{\ell_0}\int_s^{\ell_0/2} e^{\gamma\frac{(s-s')}{c}}\left\{\cos\left[\omega_n\frac{(s-s')}{c}\right]+\frac{\gamma}{\omega_n}\sin\left[\omega_n\frac{(s-s')}{c}\right]\right\}ds' =$$

$$\frac{qq_{\text{tot}}w_0c}{\ell_0\omega_n}\,e^{\gamma\frac{x}{c}}\sin\left(\omega_r\frac{x}{c}\right)\Big|_0^{s-\ell_0/2} = -\frac{qq_{\text{tot}}w_0}{2}\frac{e^{-\frac{\gamma}{c}\left(\frac{\ell_0}{2}-s\right)}\sin\left[\frac{\omega_n}{c}\left(\frac{\ell_0}{2}-s\right)\right]}{\frac{\omega_n}{c}\frac{\ell_0}{2}}.$$

Exercise 19

By using Eq. (I.12.145) with the parameters of the exercise, since $k_y = \omega_y/c$, we have

$$\frac{y_2(L_L)-\hat{y}_1}{\hat{y}_1} = \frac{cNqL_Lw_y(z)}{4\omega_y\beta^2(E_0/q)L_w} = 180.$$

The condition to neglect the beam break-up is then that

$$180\hat{y}_1 = y_2(L_L) - \hat{y}_1 \ll \sigma_y.$$

This means that, in these conditions, the beam must be injected onto the Linac axis with an accuracy better than a fraction of a per cent of the beam size.

Exercise 20

In this case, $E_f = 1 + 16.7 \times 10^{-3} \times 3000 = 51.1$ GeV, so that the multiplication factor is

$$F = \frac{E_0}{E_f} \ln \frac{E_f}{E_0} = 0.078,$$

and the amplitude of the oscillations of the tail with respect to the head becomes now

$$\frac{y_2(L_L) - \hat{y}_1}{\hat{y}_1} = 180 \times 0.078 = 14.$$

Appendices

I.12.A Effect of longitudinal distribution on the tune spread

In the left-hand side of Fig. I.12.A.1 we show the longitudinal phase space scatter plot $(\Delta\phi, \Delta E)$ of a bunch obtained by simulations for the CERN PS Booster. In the top figures, the head and tails of the bunch are represented with colors, while in the bottom ones, we have highlighted the particles in the bunch center. On the right-hand side of the figure, the corresponding tune diagram is shown. The black dot in these figures represents the bare tune.

Particles at the edges of the bunch (top figures) have tunes close to the bare tune in the necktie. Indeed, in these two longitudinal phase space regions the beam line density is smaller with respect to the centre of the bunch, therefore the space charge detuning, proportional to $\lambda(z)$ is small too.

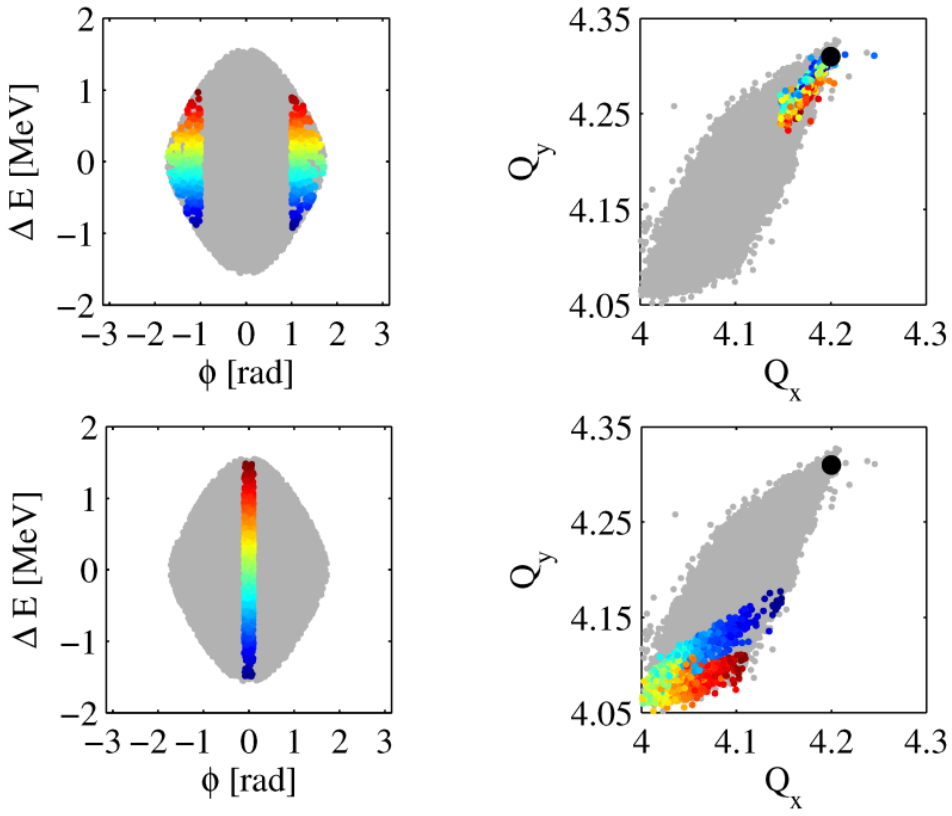

Fig. I.12.A.1: Longitudinal phase-space $(\Delta\phi, \Delta E$ scatter plot of the bunch tune footprint. (Courtesy of V. Forte [17]).

I.12.B Image charge distribution of an infinite wire inside a circular beam pipe

Let us consider the geometry of Fig. I.12.B.1. We have a direct uniform infinite linear charge distribution λ_0 at a distance x from the centre of a beam pipe of radius b. The goal is to determine the distance d from an image charge distribution $-\lambda_0$ such that the walls of the beam pipe must be equipotential.

Referring to the figure, let us evaluate the potential of the pipe wall at a distance r from the direct charge distribution and at R from the image. The same position is determined by the angle θ from the

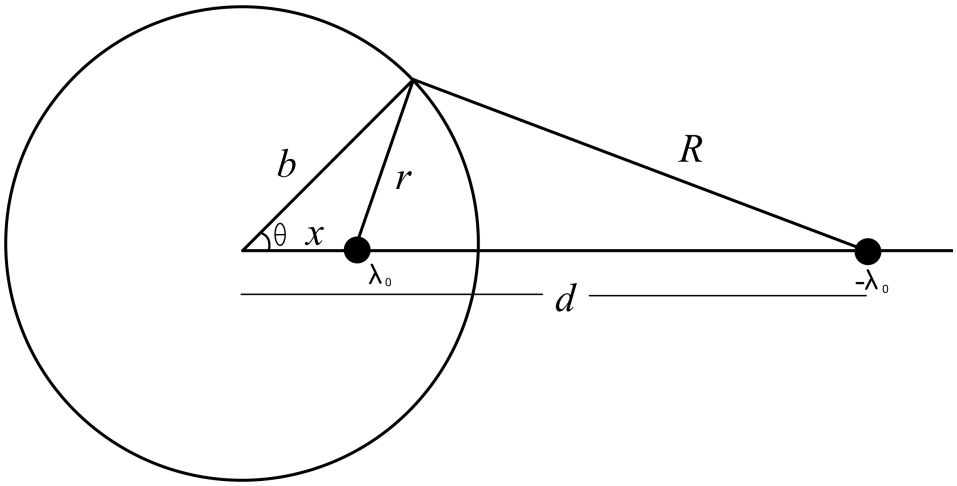

Fig. I.12.B.1: Geometry for the determination of the image charge position.

center of the beam pipe. The two distances can be written as

$$r = \sqrt{b^2 + x^2 - 2bx\cos\theta}, \tag{I.12.161}$$

$$R = \sqrt{b^2 + d^2 - 2bd\cos\theta}. \tag{I.12.162}$$

The potential produced by a uniform infinite linear distribution at a given distance r is proportional to $\lambda_0 \ln(r)$, so that the potential created by the two linear distributions must be

$$V \propto \lambda_0 \ln(r) - \lambda_0 \ln(R) = \lambda_0 \left[\ln\left(\sqrt{b^2 + x^2 - 2bx\cos\theta}\right) - \ln\left(\sqrt{b^2 + d^2 - 2bd\cos\theta}\right)\right]. \tag{I.12.163}$$

This potential must be independent from θ, so that

$$\frac{\partial V}{\partial \theta} = 0 = \frac{2bx\sin\theta}{2\left(b^2 + x^2 - 2bx\cos\theta\right)} - \frac{2bd\sin\theta}{2\left(b^2 + d^2 - 2bd\cos\theta\right)}, \tag{I.12.164}$$

that is

$$\frac{x}{\left(b^2 + x^2 - 2bx\cos\theta\right)} = \frac{d}{\left(b^2 + d^2 - 2bd\cos\theta\right)}. \tag{I.12.165}$$

This equation can be written as

$$xd^2 - d(b^2 + x^2) + xb^2 = 0. \tag{I.12.166}$$

By solving this second-order equation in d we get the two solutions

$$d_1 = x, \qquad d_2 = \frac{b^2}{x}. \tag{I.12.167}$$

Of course, the first solution gives the result that the two distributions coincide and that the electric field inside the pipe is zero everywhere, while the second solution is what we were looking for.

I.12.C Panofsky-Wenzel theorem

It is a relationship between transverse and longitudinal electromagnetic forces. It can be obtained from the properties of the Lorentz force and the impulse received by a charge with the rigid beam approximation.

It says that the transverse gradient of the longitudinal force is equal to the longitudinal gradient of the transverse force, that is

$$\nabla_\perp F_\parallel = \frac{\partial}{\partial z}\mathbf{F}_\perp,$$

which, in terms of wake function, can be written as

$$\nabla_\perp w_\parallel = \frac{\partial}{\partial z}\mathbf{w}_\perp,$$

and, in terms of impedance, as

$$Z_\perp = \frac{\beta c}{\omega}\nabla_\perp Z_\parallel.$$

I.12.D Other collective effects

Finally, we briefly list here some other important effects related to self-induced electromagnetic fields.

I.12.D.1 Landau damping

There is a fortunate stabilizing effect against the collective instabilities called "Landau Damping". The basic mechanism relies on the fact that if the particles in the beam have a spread in their natural frequencies (synchrotron or betatron), their motion can't be coherent for a long time.

I.12.D.1.1 Driven oscillators

In order to understand the physical nature of this effect, we consider a simple harmonic oscillator, at rest for $t < 0$, driven by an oscillatory force for $t > 0$, similar to what we discussed in Section I.12.3.2.1. Let us consider here the time as the independent variable so that Eq. (I.12.124) is now written as

$$\frac{d^2x}{dt^2} + \omega^2 x = A\cos(\Omega t)\,. \tag{I.12.168}$$

We have already discussed its solution when $x(0) = 0$ and $\dot{x}(0) = 0$, which now becomes

$$x(t) = \frac{A}{\omega^2 - \Omega^2}\left[\cos(\Omega t) - \cos(\omega t)\right]. \tag{I.12.169}$$

Let us now assume that the external force is driving a population of particles characterized by a spread of the natural frequencies of oscillation around the average value ω_m. Furthermore, let the forcing frequency Ω be inside the frequency spectrum. Following the same method of Section I.12.3.2.1, we can define the difference between the resonance frequency Ω and a resonator frequency ω as $\delta_\omega = \Omega - \omega$. We also suppose that $|\delta_\omega| \ll \omega_m$ such that $\Omega + \omega \simeq \omega_m$.

Under such assumptions, the above equation of motion can be written similarly to Eq. (I.12.136),

that is

$$x(t>0) = \frac{A}{\omega_m \delta_\omega} \sin(\omega_m t) \sin\left(\frac{\delta_\omega}{2} t\right). \tag{I.12.170}$$

As we have already seen, this equation can be seen as an oscillation at frequency ω_m with an amplitude modulated at the lower frequency $\delta_\omega/2$. As for Eq. (I.12.137), it is convenient to write this equation as

$$x(s) = \frac{At}{2\omega_m} \sin(\omega_m t) \frac{\sin\left(\frac{\delta_\omega t}{2}\right)}{\frac{\delta_\omega t}{2}}. \tag{I.12.171}$$

Let us now observe the option of two particles in the bunch, one with $\delta_\omega = 0$, and the other one with $\delta_\omega \neq 0$. Both are at rest and, at $t = 0$, they start to oscillate with the same amplitude and phase (coherency). However, while the amplitude of the former charge grows indefinitely since it is driven at resonance according to the blue curve of Fig. I.12.D.1, the latter, because of the beating of two close frequencies, reaches a maximum amplitude which is modulated by $\delta_\omega/2$, when $\sin(\delta_\omega t/2) = 1$, that is when $t = \pi/\delta_\omega$, after which this oscillator is out of resonance, and loses the phase synchronism with the external driving force as shown by the red curve of the same figure. We can say that the system of the particles loses the coherency at the time when the beating amplitude is maximum, i.e. for $t = \pi/\delta_\omega$.

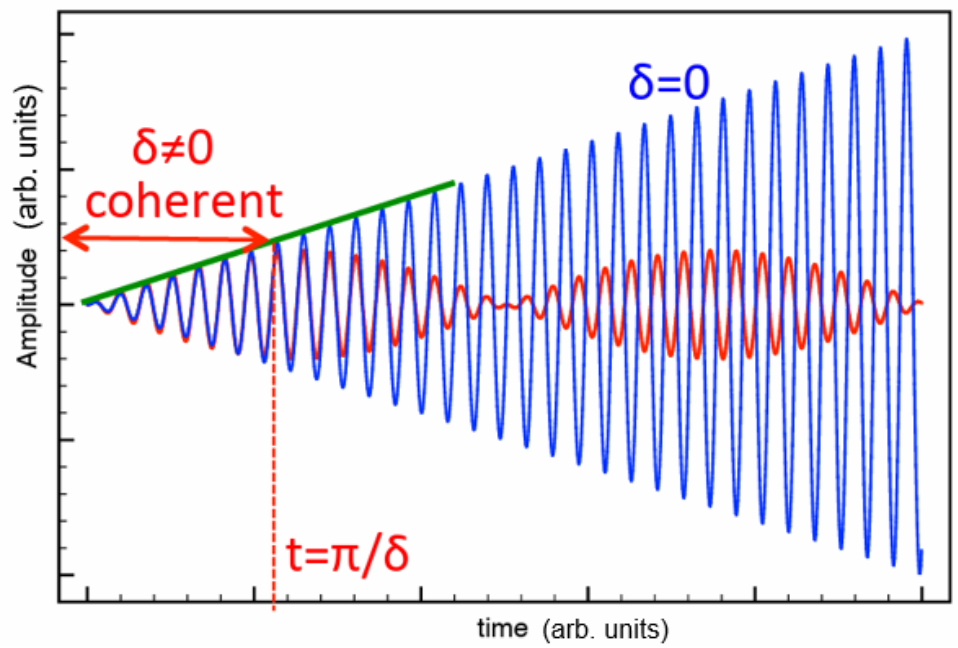

Fig. I.12.D.1: On resonance and out of resonance oscillations of two particles due to a sinusoidal external force in arbitrary units.

We can then say that at any time t^*, only those oscillators inside the bandwidth $|\delta_\omega| < \pi/t^*$ oscillate coherently. The longer we wait, the narrower the coherent bandwidth is, and therefore a lower number of particles oscillates coherently.

I.12.D.1.2 Amplitude of oscillations and energy of the system

At any instant, we can divide the bunch population into two groups: the coherent (on resonance) particles, oscillating all together with an amplitude growing linearly with time, and the incoherent (out of resonance) particles which have different phases and a saturated maximum amplitude of oscillation.

It is possible to show that, although the amplitude of the coherent oscillators grows linearly with time, the average amplitude of the whole system remains bounded. The reason is that the number of coherent particles decreases inversely with time.

As regards the energy of the system, also in this case we distinguish between the coherent and incoherent particles. The energy of the coherent particles grows quadratically with time, while the energy of the incoherent particles is bounded. In this case, although the number of coherent oscillators decreases with time, the total energy still grows linearly. This means that the system continues to absorb energy from the external driving force but the average oscillation amplitude remains bounded: when a force drives such a system, only at the beginning, the whole system follows the external force. Afterwards, fewer and fewer particles are driven at the resonance.

This mechanism also works when the driving force is produced by the bunch itself. To trigger a coherent instability, the rise time of the instability itself has to be shorter than the decoherence time of the bunch.

A rigorous analysis of the beam dynamics in the frequency domain shows that, because of the Landau damping, a stability region appears in the impedance plane, whose shape depends on the beam energy distribution.

I.12.D.2 Vlasov and Fokker-Planck equations

These equations are used to study analytically the collective effects in circular accelerators.

The Vlasov equation describes the collective behaviour of a multiparticle system under the influence of electromagnetic forces [3].

It is valid for a conservative system when we can ignore, for example, the synchrotron radiation. It is generally applied to study longitudinal and transverse beam dynamics of proton beams.

For electron beams, synchrotron radiation cannot be neglected and we need to use another equation called the Fokker-Planck equation [3, 13]. Its stationary solution in the longitudinal plane is called the Haissinski equation [18].

The Vlasov equation is sometimes loosely referred to as the Liouville theorem. However, it applies to a system of many particles when collisions among particles are excluded.

Strictly, the Liouville theorem applies to an ensemble of many systems, each containing many particles. It describes the conservation of density of the ensemble in the 2N-dimensional space and applies to situations much more general than that considered in the study of collective effects, such as when collisions among discrete particles are included.

I.12.D.3 Other effects

Here we mention some other important self-induced effects that produce beam instabilities, together with some references where the phenomenon is discussed:

- Touschek effect and intra-beam scattering [19]: Touschek effect is due to the Coulomb scattering of charged particles because of an exchange of energies between the transverse and longitudinal oscillations. Intra-beam scattering is due to multiple Coulomb scattering, leading to an increase in the beam dimensions;
- Electron cloud [20]: Positive charges disturb electrons already in the beam pipe, and bounce them into the wall. These electrons can be photo-electrons from synchrotron radiation or electrons from ionized gas molecules. When an electron hits the wall, the wall emits more electrons due to secondary emission. These electrons in turn hit the opposite wall, releasing more and more electrons into the accelerator chamber;
- Beam-beam [21]: It is due to the electromagnetic fields of two counter-rotating beams as they cross the interaction points in a collider. It can represent a severe limitation in high-intensity accelerators;
- Beam Ion instability [22]: The ionization of residual gas by an electron beam produces ions. The ions generated by the head of the bunch train oscillate in the transverse direction and resonantly interact with the betatron oscillations of the subsequent bunches, causing the growth of an initial perturbation of the beam.

References

[1] See, for example, J. Rossbach, P. Schmüser, Basic course on accelerator optics, CAS Jyväskylä 1992, CERN 94–01, p. 76, 10.5170/CERN-1994-001.17, or J.P. Delahaye *et al.*, Proc. 11th Int. Conf. on High Energy Accelerators, Geneva, 1980, pp. 299–304, CDS.

[2] L. Palumbo, V.G. Vaccaro, and M. Zobov, Wake fields and impedance, in CERN-95-06, CERN, Geneva, Switzerland, 1995, pp. 331-390 doi:10.5170/CERN-1995-006.331.

[3] A.W. Chao, *Physics of collective beam instabilities in high energy accelerators* (Wiley, New York, 1993), https://www.slac.stanford.edu/ achao/wileybook.html.

[4] K. Ng, *Physiscs of intensity dependent beam instabilities* (World Scientific, Singapore, 2002), doi:10.1142/5835.

[5] R. Boni *et al.*, DAΦNE accumulator ring coupling impedance measurements, *Nucl. Instrum. Meth. Phys. Res. A* 418 (1998), pp. 241–248, doi:10.1016/S0168-9002(98)00744-X.

[6] M. Zobov *et al.*, Collective effects and impedance study for the DAFNE PHI-Factory, LNF-95/041(P), doi:10.15161/oar.it/1448441728.54.

[7] Several papers have been dedicated to the beam break-up. An important paper that summarizes the different aspects is: A. Mosnier, in Proceedings of the CAS-CERN Accelerator School: 5th Advanced Accelerator Physics Course, Rhodes, Greece, 20 September–1 October 1993, CERN-1995-006 (CERN, Geneva, 1995), pp. 459–514, doi:10.5170/CERN-1995-006.459.

[8] H. Altenmueller *et al.*, Beam break-up experiments at SLAC, SLAC-PUB-224 (1966), Inspire.

[9] V.E. Balakin, A.V. Novokhatsky, and V.P. Smirnov, VLEPP: transverse beam dynamics, in Proc. of the 12th Int. Conf. on High Energy Accelerators, Fermilab, (1983), pp. 119–120, Inspire.

[10] V.G. Vaccaro, Longitudinal instability of a coasting beam above transition, due to the action of lumped discontinuities, CERN-ISR-RF-66-35, 1966, CDS.

[11] A.M. Sessler and V.G. Vaccaro, Longitudinal instabilities of azimuthally uniform beams in circular vacuum chambers with walls of arbitrary electrical properties, CERN 67-2, 1967, doi:10.5170/CERN-1967-002.

[12] A.A. Vlasov, Many-particles theory and its application to plasma, State Publishing House, Moscow, 1950; English translation 1961, Internet Archiv.

[13] C. Bernardini, and B. Touschek, On the quantum losses in an electron synchrotron, Laboratori Nazionali di Frascati del CNEN, Nota interna No. 34 (1960), doi:10.15161/oar.it/1447934041.29.

[14] E. Métral, Proc. 10th Int. Particle Accelerator Conf. IPAC2019, Melbourne, Australia, 19–24 May 2019, pp. 312–315, doi:10.18429/JACoW-IPAC2019-MOPGW087.

[15] N. Mounet, "DELPHI: an analytic Vlasov solver for impedance-driven modes" (2014), CERN-ACC-SLIDES-2014- 0066 CDS.

[16] G. Rumolo and F. Zimmermann, *Phys. Rev. ST Accel. Beams* **5** (2002) 121002, doi:10.1103/PhysRevSTAB.5.121002; N. Mounet, Ph.D. thesis, EPFL, Lausanne, Switzerland, (2012), CDS; G. Bassi, A. Blednykh, and V. Smaluk, *Phys. Rev. Accel. Beams* **19** (2016) , doi:10.1103/PhysRevAccelBeams.19.024401; M. Migliorati, L. Palumbo, *Phys. Rev. ST Accel. Beams* **18** (2015) 031001, doi:10.1103/PhysRevSTAB.18.031001; D. Quartullo *et al.*, Proc. HB2016, Malmö, Sweden, July 2016, pp. 140–145, CDS; R.D. Ryne, Advanced computing tools and models for accelerator physics, in Proc. EPAC08, Genoa, Italy, JACoW.

[17] V. Forte, Performance of the CERN PSB at 160 MeV with H- charge exchange injection, Ph.D. thesis, Université Blaise Pascal, Clermont-Ferrand, France, 2016, CDS.

[18] J. Haïssinski, Exact longitudinal equilibrium distribution of stored electrons in the presence of self-fields, *Nuovo Cim. B* **18** (1973) 72–82, https://doi.org/10.1007/BF02832640.

[19] A. Wrülich, CERN 94-01, Vol. I, pp. 409–435, doi:10.5170/CERN-1994-001.409.

[20] G. Iadarola, Electron cloud studies for CERN particle accelerators and simulation code development, Ph.D. thesis , Università degli Studi di Napoli Federico II, Napoli, Italy, March 2014, CDS.

[21] H. Mais, C. Mari, CERN 94-01, Vol. 2, pp. 499–524 , doi:10.5170/CERN-1994-001.499.

[22] G. V. Stupakov, A Fast Beam-Ion Instability, SLAC-PUB-10377, Inspire.